REPORT SERIES IN AEROSOL SCIENCE
N:o 230 (2020)

PRECIPITATION CONTROLS ON CARBON AND WATER RELATIONS IN TWO AFRICAN ECOSYSTEMS

MATTI RÄSÄNEN

Institute for Atmospheric and Earth System Research / Physics
Faculty of Science
University of Helsinki
Helsinki, Finland

Academic dissertation

To be presented, with the permission of the Faculty of Science of the University of Helsinki, for public criticism in auditorium D101, Gustaf Hällströmin katu 2, on September 3rd, 2020, at 1 o'clock in the afternoon.

Helsinki 2020

Author's Address: Institute for Atmospheric and Earth System Research / Physics
P.O. Box 64
FI-00014 University of Helsinki
matti.rasanen@helsinki.fi

Supervisors: Academician Markku Kulmala, Ph.D.
Institute for Atmospheric and Earth System Research / Physics
University of Helsinki

Professor Janne Rinne, Ph.D.
Department of Physical Geography and Ecosystem Science
Lund University

Professor Petri Pellikka, Ph.D.
Department of Geosciences and Geography
University of Helsinki

Reviewers: Docent Tuula Aalto, Ph.D.
Finnish Meteorological Institute

Associate Professor Ari Laurén, Ph.D.
School of Forest Sciences
University of Eastern Finland

Opponent: Associate Professor Stefano Manzoni, Ph.D.
Department of Physical Geography
Stockholm University

ISBN 978-952-7276-41-9 (printed version)
ISSN 0784-3496
Helsinki 2020
Unigrafia Oy

ISBN 978-952-7276-43-3 (pdf version)
http://ethesis.helsinki.fi
Helsinki 2020
Helsingin yliopiston verkkojulkaisut

Behind us, beyond us now
is phantom territory, a world
abstract as memories of earth
the traveling dead take home.
Between obscuring cloud
and cloud, the cloudy dark
ensphering us seems all we can
be certain of. Is Plato's cave.

Robert Hayden
Traveling through Fog, 1972

Acknowledgements

This thesis was carried out at the Institute of Earth System and Atmospheric Research (INAR) of the University of Helsinki. I acknowledge the support from the TAITAWATER and SMARTLAND projects funded by the Academy of Finland. The Taita Research Station of the University of Helsinki is acknowledged for the help in the fieldwork in Kenya. I want to thank Academician Markku Kulmala for accepting me as a student and providing a stimulating working environment. I also want to thank Docent Tuula Aalto and Associate Professor Ari Laurén for pre-examining this thesis and Associate Professor Stefano Manzoni for serving as an opponent for the defense.

I want to thank Professor Gabriel Katul for the close collaboration and a pleasant and exciting visit to Duke University. Your nurturing attitude in mentoring and fulgurant presence made this possible. Many thanks to Professor Ram Oren for the needed astuteness at the end of the work. I also want to thank Professor Janne Rinne for sharing the excitement in the fieldwork and early stages of the research and Professor Petri Pellikka for the support and organization of the research in Kenya.

I thank all the coauthors for the support in manuscript preparation and for carrying out the measurements. Thank you to all my colleagues at various departments. I thank Lauri Laakso and the NWU team for the chance to work in South Africa. I also thank Erkki Siivola for the support in experimentation. I am grateful for Antti and Sheila, for our thoughtful discussions. Thank you Juuso for the great teamwork. A special thanks to Ekaterina for valuable comments on the thesis. Thank you to the wonderful staff at the Taita Research station. And, especially, thanks to Ken, Mwadime, and Darius for the physical and spiritual heavy lifting during the fieldwork. *Pamoja!*

Finally, thanks to my relatives and friends for all the support. My deepest gratitude is to Marinka for sharing the joy and making it all worthwhile. Above all, thanks to our children for showing the world anew.

Matti Tapio Räsänen
University of Helsinki, 2020

Abstract

Understanding the interaction between precipitation and vegetation growth in water-limited ecosystems is vital for various livelihoods that depend on water resources. Precipitation is the primary driver of vegetation growth in dry ecosystems, while fog deposition is essential for the microclimate at dry coastal ecosystems and cloud forests. The analysis of soil moisture, which incorporates the action of climate, soil, and vegetation, is the key to understanding the carbon and water relations and the interaction between precipitation and vegetation.

This thesis examines the impacts of precipitation variability on carbon and water relations in African savannas and the similarities in rainfall and fog deposition. The ecosystem-scale transpiration was estimated from eddy covariance measurements based on annually fitted water use efficiency and optimality hypothesis. The soil moisture measurements were analyzed using a hierarchy of soil moisture models with precipitation, NDVI, and potential evapotranspiration (PET) variability. The statistics of fog and rainfall were analyzed using an analogy with self-organized criticality.

The annual evapotranspiration (ET) was comparable to the annual precipitation at the grazed savanna grassland. While the annual precipitation was highly variable, the estimated annual transpiration was nearly constant 55 % of ET. The transpiration (T) was reduced only during the drought year due to grass dieback-regrowth and possibly due to other changes in soil surface properties that enhanced evaporation. The annual net CO_2 exchange (NEE) had large variation ranging from –58 (sink) to 198 (source) $\mathrm{gC\,m^{-2}\,yr^{-1}}$. The annual NEE was related to the maximum of remotely sensed vegetation index (NDVI), and the annual ecosystem respiration was strongly correlated with early season rainfall amount. The analysis of measured soil moisture across savannas showed that NDVI and PET adjustments to daily maximum ET are necessary for modeling depth averaged soil moisture. The soil moisture memory timescale, a rough measure of the time it takes for a soil column to forget the initial soil moisture state, was linearly related to daily mean precipitation intensity at semi-arid savannas.

Both rainfall and fog time series showed approximate power-law relations for dry period and event size distributions consistent with self-organized criticality prediction. The spectral exponents of the on-off time series of the fog and rainfall exhibited an

approximate $f^{-0.8}$ scaling, but the on-off switching was not entirely independent from the amplitude intermittency in fog and rainfall.

The results show the role of short and long-term variability in precipitation and its consequences for the carbon and water cycle of semi-arid savannas with significant tree cover. These findings can be used to develop minimalist water balance models to understand how vegetation state affects water resources.

Keywords: savanna, soil moisture, transpiration, carbon balance, rainfall intermittency, fog deposition

Contents

List of publications

This thesis consists of an introductory review, followed by four research articles. In the introductory part, the papers are cited according to their roman numerals. **Papers I–III** are reprinted under the Creative Commons Attribution License. **Paper IV** is reprinted with permission from John Wiley and Sons.

I **Räsänen, M.**, Aurela, M., Vakkari, V., Beukes, J. P., Tuovinen, J.-P., Zyl, P. G. V., Josipovic, M., Siebert, S. J., Laurila, T., Kulmala, M., Laakso, L., Rinne, J., Oren, R. and Katul, G. (2020). The effect of rainfall amount and timing on annual transpiration in grazed savanna grassland, *Hydrology and Earth System Sciences Discussions*, 1–31.

II **Räsänen, M.**, Aurela, M., Vakkari, V., Beukes, J. P., Tuovinen, J.-P., Van Zyl, P. G., Josipovic, M., Venter, A. D., Jaars, K., Siebert, S. J., Laurila, T., Rinne, J. and Laakso, L. (2017). Carbon balance of a grazed savanna grassland ecosystem in South Africa, *Biogeosciences*, 14(5), 1039–1054.

III **Räsänen, M.**, Merbold, L., Vakkari, V., Aurela, M., Laakso, L., Beukes, J.P., Van Zyl, P.G., Josipovic, M., Feig, G., Pellikka, P., Rinne, J., and Katul, G.G. (2020). Root-zone soil moisture variability across African savannas: From pulsed rainfall to landcover switches. *Ecohydrology*, 13(5), 1–20.

IV **Räsänen, M.**, Chung, M., Katurji, M., Pellikka, P., Rinne, J. and Katul, G. G. (2018). Similarity in fog and rainfall intermittency, *Geophysical Research Letters*, 45(19), 10–691.

Author's contribution

	I	II	III	IV
Conceptualization	MR,CO	MR,CO	MR,CO	MR,CO
Methodology	MR,CO	MR,CO	MR,CO	MR,CO
Measurements	CO	CO	MR,CO	MR,CO
Data post-processing	MR,CO	MR,CO	MR	MR
Formal analysis and visualization	MR	MR	MR	MR
Writing the initial draft	MR	MR	MR	MR
Review and revision	MR,CO	MR,CO	MR,CO	MR,CO

MR=Matti Räsänen and CO=Coauthors

1 Introduction

Understanding the interaction between precipitation and vegetation growth in water-limited ecosystems is important for various livelihoods that depend on water resources. It is essential for example in rainfed agriculture (Vico and Porporato, 2011), management of grazing and conservation areas (Sankaran et al., 2005) and tree planting (Enku et al., 2020). Precipitation is the primary driver of vegetation growth in water-limited ecosystems. In arid and semi-arid ecosystems, the evapotranspiration (ET) is large due to high incoming radiation, and ET can be comparable to precipitation amount at annual scales. The surface soil moisture is the key variable linking precipitation and ET. The atmosphere may also be strongly coupled to the land surface at African savannas where the soil moisture state exerts control over rainfall formation (Green et al., 2017; Koster et al., 2004).

The African savanna ecosystems organize to patchy landscapes roughly consisting of areas of bare soil, grasses, and trees. The savanna grasses use the C_4 photosynthetic pathway and are intensive users of surface soil water, whereas trees use the C_3 pathway and are conservative water users (Scholes and Archer, 1997; Bond, 2008). Much research on the codominance of trees and grasses has focused on the rooting-depth separation of grasses and trees (Walker and Noy-Meir, 1982; Ward et al., 2013), but the difference in leaf phenology of trees and grasses is also an important factor in tree-grass coexistence. Many savanna tree species can make new leaves before the first rains, while the grass layer phenology follows the rainfall (Whitecross et al., 2016; Archibald and Scholes, 2007). Trees can use the first rains for photosynthesis, which is not possible for the grass layer that regrows every year. This way, the trees and grasses take up water from different soil volumes and during different times due to the leaf phenology (Scholes and Walker, H., 1993).

The surface soil moisture is the outcome of the hydrological fluxes, including precipitation, deep drainage, runoff, and ET. Deep drainage can be significant for wet savannas, whereas, at dry savannas, the water loss from the soil is dominated by ET (Miller et al., 2012). Part of precipitation can evaporate as interception before it reaches the soil, and it contributes directly to the evaporation flux. The transpiration (T) component of ET is linked to the carbon uptake of the vegetation. Transpiration is nearly constant when soil is wet (no water stress) and linearly decreasing with soil moisture during water-stress periods (Laio et al., 2001). The time series of water-stress and non-stress

periods enable to study the distribution of dry periods. These water stress periods are nonlinearly related to the precipitation frequency (Porporato et al., 2001).

The carbon balance of savanna ecosystems is governed by various factors such as vegetation structure, physiology, phenology, and the pulsed nature of rainfall (Hill and Hanan, 2011). The annual sum of net ecosystem exchange (NEE) has been observed to range between –429 (sink) and +155 (source) $\mathrm{gC\,m^{-2}\,yr^{-1}}$ across sites in semi-arid African savannas (Ago et al., 2014; Archibald et al., 2009; Brümmer et al., 2008; Quansah et al., 2015; Tagesson et al., 2015; Veenendaal et al., 2004). At South African savanna, Archibald et al. (2009) found that main drivers of interannual variation in NEE were the amount of absorbed photosynthetically active radiation, the length of the growing season and the number of days in the year when moisture was available in the soil. Across the Sahel, the variability of NEE was strongly linked to changes in gross primary production (GPP), which was regulated by vegetation phenology and soil moisture dynamics (Tagesson et al., 2016).

At savanna ecosystems, soil dries fast between rainfall events, resulting in a pulse-driven system that affects the carbon fluxes (Huxman et al., 2004). The ecosystem respiration consists of the autotrophic respiration from leaves and roots and the heterotrophic respiration mostly from decomposition of soil organic matter by soil micro-organisms. Both of these processes are temperature and soil moisture dependent. The ecosystem respiration and photosynthesis have a different response time to the pulses of rainfall. For example, at the Skukuza site in South Africa, the respiration reached a maximum 1–3 days after rainfall events, while maximum photosynthesis occurred up to 9 days after soil wetting (Hill and Hanan, 2011).

The pulsed nature of rainfall can be studied by the rain/no-rain time series that captures the switching states similarly to the switching of water stress/no stress periods of soil moisture. This rainfall intermittency is one of the key uncertainties in rainfall forecasting (Rigby and Porporato, 2010). The change in precipitation frequency is also the main difference in precipitation statistics, for example, in the Kalahari transect of savannas where annual precipitation ranges from 300 to 950 $\mathrm{mm\,yr^{-1}}$. One precipitation event occurs on average every 11 days to every three days across the transect, whereas the mean daily amount of rainfall is near-constant 10 $\mathrm{mm\,day^{-1}}$ (Porporato et al., 2003).

The rainfall statistics have been studied from the point of view of complexity and self-organization theory (Peters et al., 2001; Peters and Neelin, 2006; Yano et al., 2012). Rainfall can be viewed as a second-order phase transition where the no rain periods (off phases) are ordered, but the rain-on phases are disordered. At a large spatial scale, the precipitation event resembles a disordered state because the two phases can spatially coexist, and thus the boundary delineating the two phases need not be discontinuous at a precipitation event scale. Certain mean meteorological variables can act as control parameters favoring the switching between the ordered and disordered states. A prototypical model for such phase transition is self-organized criticality (SOC), which has been studied in the context of rainfall (Peters and Christensen, 2006; Peters et al., 2010). The rainfall event size, event duration, and dry period distributions often exhibit a power-law scaling that is a necessary but not sufficient condition for SOC to hold (Peters et al., 2010).

In this thesis, a comparison of rainfall and fog intermittency was made to better understand the relation between these processes. Fog occurrence is important for several microclimates such as western continental margins, montane cloud forests, and several deserts (Bruijnzeel et al., 2005; Garreaud et al., 2008; Kaseke et al., 2017). In the East African landscape, there are mountains that receive high rainfall, and fog occurs often. Frequent fog occurrence leads to a cool and humid environment with reduced transpiration rates and wet soils, thereby supporting water demands for photosynthesis. The cloud forests are hotspots of biodiversity, and the role of fog is fundamental for these forests. The advective fog originates from the ocean, while the radiation fog is a local phenomenon. Advective fog is common at the western continental margins (Garreaud et al., 2008), but in desert locations, the local radiation fog can be as frequent as advective fog (Kaseke et al., 2017). The analysis of fog intermittency and its connection to rainfall is an important step in understanding the possible similarities in their statistical structure. These connections and the fog statistics may help to formulate stochastic simulation of fog events and test whether detailed physical models reproduce the observed fog statistics. Moreover, these results may offer clues about the dynamics governing fog formation at a particular range of temporal scales.

This thesis aims to uncover the precipitation impacts on carbon and water relations in savannas. The multiyear measurements reveal the short and long term variability of vegetation and hydrologic state and their relation to precipitation variability. These observations are essential in the further development of ecohydrological theory.

The specific research questions and aims are:

- To quantify carbon and water balance for a grazed savanna grassland. How ET and its components (T and E) vary with annual precipitation and vegetation changes? (**Paper I**, **Paper III**)
- What explains the high variability of annual carbon balance for grassland savanna? (**Paper II**)
- To quantify precipitation and soil moisture variability across savannas. What explains the mean root-zone soil moisture variability? How are long dry periods distributed? (**Paper III**)
- To explore the similarity of rainfall and fog statistics. Are the on-off switching properties of rainfall and fog similar? (**Paper IV**)

2 Materials and methods

2.1 Eddy covariance measurements

The exchange of heat and mass between the atmosphere and land surface is due to turbulent transport in the atmospheric boundary layer (ABL). The turbulent transport is mostly produced by frictional drag producing wind shear and by surface heating producing buoyant turbulence (Stull, 1988). Typically, the ABL height is 1–2 km on land. The atmospheric surface layer, covering 10% of the ABL height near the surface, is the most relevant for the surface exchange measurements. It is also called the constant flux layer because fluxes are assumed to be approximately constant with height within this layer (Foken, 2017). The lowest parts of the constant flux layer are the canopy layer corresponding to canopy height and the roughness sublayer that is roughly twice the canopy height. The eddy covariance measurements are done above roughness sublayer by high frequency measurements of wind velocity and concentration of transported quantity such as water vapor and CO_2.

The eddy covariance measurement is a direct measurement of the half-hour average ecosystem-scale flux. By assuming horizontal homogeneity and stationary turbulence statistics, the equation for mass conservation in the eddy covariance technique can be expressed as

$$F_s = \overline{\rho_d}\overline{w'\chi_s'}\Big|_h + \int_0^{z_m} \overline{\rho_d}\overline{\frac{\partial \chi_s}{\partial t}} dz \,, \tag{1}$$

where F_s is flux of scalar s, ρ_d is the dry air density, w' is the vertical wind fluctuations around the mean and χ_s is the mixing ratio of scalar s (Aubinet et al., 2012). The second term on the right-hand side is the storage change term, which represents the changes in χ_s below the measurement height. It may be negligible for latent heat flux but is usually accounted for carbon dioxide flux. The consequence of the assumptions made is that the quality of the eddy covariance method at given times is affected by the measurement location, the characteristics of the instruments and turbulent flow.

The source area for eddy covariance measurement can be estimated using a flux footprint model that parametrizes the boundary layer mixing (Vesala et al., 2008; Leclerc and Foken, 2014). It is important to estimate the footprint area and verify that it corresponds to a flat and homogeneous area for all flow conditions. For the savanna grassland analysis, the mean 80 % cumulative flux footprint area was predominantly

located within homogeneous thornveld (**Paper I**). In the grazed savanna grassland, the carbon dioxide storage was calculated by assuming a uniform distribution of CO_2 (**Paper I**).

In stable conditions, the measured CO_2 flux can be underestimated, and it is diagnosed by flux dependence on the friction velocity (u*) (Aubinet et al., 2012). This is typically solved by rejecting night-time CO_2 flux measurements that fall below critical u* value (Goulden et al., 1996). The u* threshold was estimated to be 0.28 $\mathrm{m\,s^{-1}}$ for the whole data set using a bootstrap technique from 200 artificial replicates of the data set (Wutzler et al., 2018). The heat flux and NEE values were discarded when u* was below this threshold. The details of eddy covariance processing steps are presented in **Paper I** and **Paper II**.

The uncertainty for annual carbon balance and annual ET was estimated by considering the most significant but not necessarily all possible random and systematic errors. The uncertainty of carbon balance included estimating random error, gapfill error, and error due to spectral correction (**Paper II**). The annual ET error included random error and error due to u* filtering. For both carbon and ET uncertainty, the u* error was estimated as detailed in **Paper I**.

2.1.1 Partitioning of carbon flux

The eddy covariance method directly measures the net ecosystem exchange (NEE) of carbon dioxide. The NEE is equal to the sum of two large but opposing fluxes:

$$\mathrm{NEE} = \mathrm{R_{eco}} - \mathrm{GPP}\,, \tag{2}$$

where $\mathrm{R_{eco}}$ is the ecosystem respiration and GPP is the gross primary productivity. Here the flux from the atmosphere to plants is negative. The partitioning of CO_2 flux was done in a moving window by estimating ecosystem respiration by night-time mean and GPP as the difference between NEE and ecosystem respiration. The missing values in the GPP time series were filled with the GPP values calculated from light response curves (**Paper II**). The moving data window was defined for each day with an initial length of 6 days and expanded up to 20 days if necessary to include at least 50 points (**Paper II**).

The annual NEE was not sensitive to the gapfilling routines tested here. The mean of annual respiration based on night-time mean respiration was 82 $\mathrm{gC\,m^{-2}\,yr^{-1}}$ larger

than the annual respiration gapfilled with exponential temperature dependence used in **Paper II**. However, the mean annual NEE based on night-time mean respiration was only 26 $\mathrm{gC\,m^{-2}\,yr^{-1}}$ larger than the mean annual NEE based on the exponential temperature dependence. This difference in the mean annual NEE is similar to the annual NEE uncertainties (Table 2). Other gapfilling routines have been used at savannas, including Poisson temperature function and artificial neural network approach (Isaac et al., 2017; Archibald et al., 2009). Here the moving window approach was used due to relatively short gaps in the data.

2.1.2 Partitioning of evapotranspiration

Three methods were tested for partitioning of ET to its components transpiration (T) and evaporation (E) in **Paper I**. These methods are premised on the fact that GPP is linked through stomatal exchange of CO_2 for water vapor to transpiration component of ET. The flux-based water use efficiency is defined as

$$\mathrm{WUE} = (\mathrm{GPP/T}) = \frac{\mathrm{c_a}}{1.6\mathrm{VPD}}\left(1 - \frac{\mathrm{c_i}}{\mathrm{c_a}}\right), \tag{3}$$

where c_i and c_a are the intercellular and ambient atmospheric CO_2 concentration and VPD is the vapor pressure deficit (Katul et al., 2009). Here the leaf level difference between partial pressures has been replaced with VPD. When the equations of leaf level exchange of CO_2 and water vapor are solved by assuming that plants minimize water loss and maximize carbon gain, the dependence of c_i/c_a ratio on VPD is expressed as

$$1 - \frac{\mathrm{c_i}}{\mathrm{c_a}} \approx \left(\frac{1.6\lambda_\mathrm{L}}{\mathrm{c_a}}\right)^{1/2}\sqrt{\mathrm{VPD}}\,, \tag{4}$$

where λ_L is the marginal water use efficiency (or the Lagrange multiplier in optimal stomatal theories) (Katul et al., 2009). The equation 3 and 4 can be combined to expression:

$$\frac{\mathrm{GPP}\times\sqrt{\mathrm{VPD}}}{\mathrm{T}} = \sqrt{\frac{\mathrm{c_a}\lambda_\mathrm{L}}{1.6}}\,, \tag{5}$$

where the right-hand side of the equation is assumed essentially constant for a given vegetation type assuming c_a does not vary appreciably. The linear scaling of $\mathrm{GPP}\times\sqrt{\mathrm{VPD}}$ and ET has been noted at multiple sites and it is used to infer the relationship between GPP and T (Zhou et al., 2014; Berkelhammer et al., 2016).

The estimated transpiration from the Berkelhammer method is presented in this thesis. It was deemed most plausible and used in the final water balance analysis in **Paper I**. This method was applied to each year individually due to large changes in vegetation phenology between the years. In the Berkelhammer method, the T=ET line is empirically established by fitting a line to the minimum ET values (fifth percentile) and GPP $\times$ VPD$^{0.5}$ bins (Berkelhammer et al., 2016). For each equal-sized GPP $\times$ VPD$^{0.5}$ bin, the fifth percentile of ET defines the point where T=ET. A linear regression of these fifth percentile points defines the T=ET line, and any point below this line has T/ET equal to 1.0 by definition. For other half-hour points, the T/ET is defined as

$$\frac{\mathrm{T}}{\mathrm{ET}} = \frac{min_{GPP}||\mathrm{ET}||}{\mathrm{ET_{flux}}}\,, \tag{6}$$

where $min_{GPP}||\mathrm{ET}||$ is the minimum ET value calculated from the fit of T=ET line and $\mathrm{ET_{flux}}$ is the observed ET value. The calculation of half-hour T/ET values is illustrated in Figure 1. The monthly T/ET values were calculated by taking the mean of all half-hour T/ET values within the month.

2.2 Root-zone water balance

The mean root-zone water balance can be expressed as:

$$\eta Z_r \frac{ds(t)}{dt} = \gamma \mathrm{P(t)} - \mathrm{ET(t)} - \mathrm{D_r(t)} = \gamma \mathrm{P(t)} - \mathrm{L(t)}\,, \tag{7}$$

where s is the depth average root-zone soil moisture, η is the soil porosity, Z_r is the mean root-zone depth, γ is a constant that depends on interception loss, P is precipitation, ET is evapotranspiration, $\mathrm{D_r}$ is subsurface drainage, and L includes all the loss terms. This equation describes the change in the mean amount of water in the root-zone assuming that root-water uptake equals transpiration and assuming no horizontal water movement. The soil moisture sensors measure volumetric water content ($\mathrm{m^3\,m^{-3}}$). The depth average root-zone soil moisture (s) is calculated by taking the average of volumetric water content values in depth and dividing it with porosity. The γ was estimated as a constant that represents interception, re-evaporation and any spatial mismatch between rainfall and soil moisture (**Paper III**). The γ value for each site was determined as the slope of linear regression between cumulative soil moisture increases and cumulative precipitation. The soil moisture increases were determined from the start of the precipitation event to 24 hours after the end of the precipitation

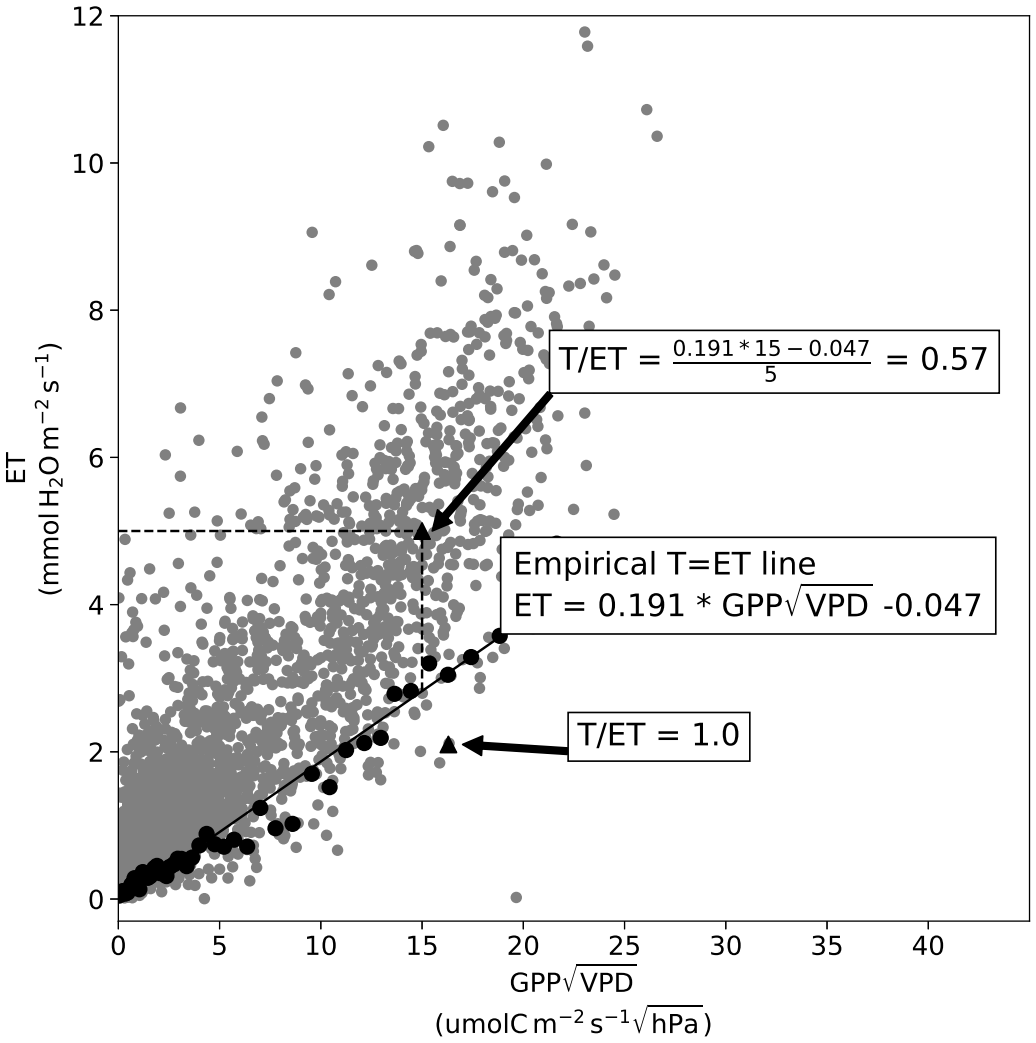

Figure 1: A fit of an annual T=ET line and an example calculation of half-hour T/ET values for points indicated by triangles. The gray circles indicate all half-hour values, and black dots indicate fifth percentile points of each GPP $\times$ $\text{VPD}^{0.5}$ bin. The empirical T=ET line is a linear fit to the fifth percentile points.

event. This approach does not consider non-linear changes in the interception loss due to storm characteristics.

A hierarchy of models was used in order to understand the contribution of precipitation, Normalized Difference Vegetation Index (NDVI) and potential evapotranspiration (PET) on the temporal soil moisture variability (**Paper III**). In model 1, the maximum daily ET is held constant, and thus only rainfall variability induces temporal variability in soil moisture values. This model has been widely used in the analysis of soil moisture variability in semi-arid ecosystems using daily time steps (Porporato et al., 2001). In model 2, the maximum daily ET is adjusted by NDVI, which represents seasonal leaf area changes. Model 3 has an additional effect of PET at seasonal and diurnal scales to the maximum daily ET. This mean root-zone model approach has also been compared to a vertically explicit solution to Richards' equation, and the two models are similar if plants are able to compensate for the root water uptake between wet and dry regions (Guswa et al., 2002).

The model 1 has constant E_{max} loss adjusted by soil moisture given by (Laio et al., 2001):

$$\mathrm{L} = \mathrm{ET} + \mathrm{D_r} = \begin{cases} 0, & s \leq s_w, \\ E_{max}\frac{s-s_w}{s_*-s_w}, & s_w < s \leq s_*, \\ E_{max}, & s_* \leq s \leq s_{fc}, \\ E_{max} + K_{sat}\left(\frac{s-s_{fc}}{1.0-s_{fc}}\right)^c, & s_{fc} \leq s \leq 1, \end{cases} \tag{8}$$

where s_w is the wilting point, s^* is the water-stress point, s_{fc} is the field capacity and the subsurface drainage below the rooting zone is represented by a saturated hydraulic conductivity K_{sat} and an exponent c that varies with soil type (or pore structure), and E_{max} is maximum evapotranspiration. The constant E_{max} and s^* were estimated from the incipient point where eddy covariance measured maximum daily ET begins to decline with decreasing s. In summary, the losses from the root-zone are nonlinear during the drainage when soil moisture is higher than the field capacity, constant between field capacity and water-stress point and linearly decreasing with soil moisture below the water-stress point.

In model 2 the maximum daily evapotranspiration varies with NDVI (Yin et al., 2014) as

$$E_{max} = a_2\left[1 - \exp\left(-b\mathrm{NDVI}\right)\right], \tag{9}$$

where a_2 is a fitting parameter and the b parameter is an extinction coefficient for global radiation set to 0.4 for models 2 and 3 (Al-Kaisi et al., 1989; Teuling et al., 2006). The NDVI time series was generated at each site based on MODIS collection 6 NDVI 250 m product (MOD13Q1) (Didan, 2015). The original 16-day interval time series was smoothed using Savitzky-Golay filter and linearly interpolated to one-hour time step for model 2 and model 3 (Isaac et al., 2017).

Finally, the model 3 further expands on model 2 by allowing a radiation-based potential evapotranspiration and NDVI to jointly impact maximum evapotranspiration rate at sub-hourly time scale:

$$E_{max} = a_3 \left[1 - \exp\left(-b\mathrm{NDVI}\right)\right] \mathrm{PET}\,, \tag{10}$$

where a_3 is a fitting parameter and PET is determined (at sub-hourly time scales) using the Priestley-Taylor formulation (Priestley and Taylor, 1972):

$$\mathrm{PET} = \alpha_{PT} \frac{\Delta}{\Delta + \gamma_p} (\mathrm{Rn} - \mathrm{G})\,, \tag{11}$$

where $\alpha_{PT} = 1.26$ is the Priestley-Taylor coefficient, Δ is the slope of the Clausius-Clayperon equation with respect to temperature evaluated at the measured air temperature, γ_p is the psychrometric constant, Rn is net radiation and G is soil heat flux. The details of the model parameter fitting are given in **Paper III**.

2.3 Soil moisture memory

The storage term $(\mathrm{d}s(t)/\mathrm{d}t)$ in Eq. 7 is linked to the storage of soil water in the pores and it introduces memory into the soil moisture. This memory is represented by the slow decay of autocorrelation function of the soil moisture time series and it is calculated as the integral timescale of the autocorrelation function (Priestley, 1981):

$$\rho_s(t, \delta) = \frac{\overline{s'(t)s'(t+\delta)}}{\sigma_s^2}\,, \tag{12}$$

where ρ_s is the autocorrelation, s refers to soil moisture series, primes denote fluctuations around the mean, δ is the time lag and σ_s^2 is the variance of soil moisture. The memory time scale is the area under the autocorrelation function

$$\tau = \int_0^{+\infty} \rho_s(\delta) \mathrm{d}\delta. \tag{13}$$

when stationarity is assumed for the autocorrelation function. The relation between soil moisture, autocorrelation, and memory timescale is illustrated in Fig. 2. If the precipitation in the lumped water balance (Eq. 7) is a white noise process and the ET losses are linearly related to soil moisture state, then the soil moisture memory can be analytically predicted to be $(\eta Z_r)/E_{max}$ (Nakai et al., 2014). This means that the size of the soil water storage (ηZ_r) and E_{max} control the memory timescale.

2.4 Time series analysis

Precipitation, fog deposition, and root-zone soil moisture time series were analyzed over different timescales using methods that have been used to study rainfall intermittency (Molini et al., 2009) and root-zone soil moisture dynamics of forests (Ghannam et al., 2016).

The on-off switching of rainfall and fog was studied using the telegraphic approximation (TA) which contains no information about magnitude variation. For time series $s(t)$ representing fog deposition, rainfall, or soil moisture the TA time series is calculated by the following equation:

$$TA(s(t)) = \frac{1}{2}\left[\frac{s(t) - s^*}{|s(t) - s^*|} + 1\right], \tag{14}$$

where s^* is a threshold to be exceeded. For fog and rainfall s^* is set to zero and for the root-zone soil moisture the s^* is equal to the water-stress point (s^* in Eq. 8). Because $TA(s(t))$ is a binary series composed of either 1 or 0 in time, it only preserves the on-off or off-on switching in $s(t)$ but contains no information about magnitude variation.

The power spectrum of rainfall, fog deposition, and soil moisture was calculated for normalized time series as follows:

$$s_n(t) = \frac{s(t) - \overline{s(t)}}{\sigma_s}, \tag{15}$$

where $\overline{s(t)}$ is the mean and σ_s is the standard deviation of series $s(t)$. All the spectra were estimated using the Welch-averaged modified periodogram method (Welch, 1967). For fog and rainfall analysis the window length was set to a quarter of the time series length. For the soil moisture analysis, the window length varied from 130 to 268 days for the different measurement sites depending on the measurement record duration.

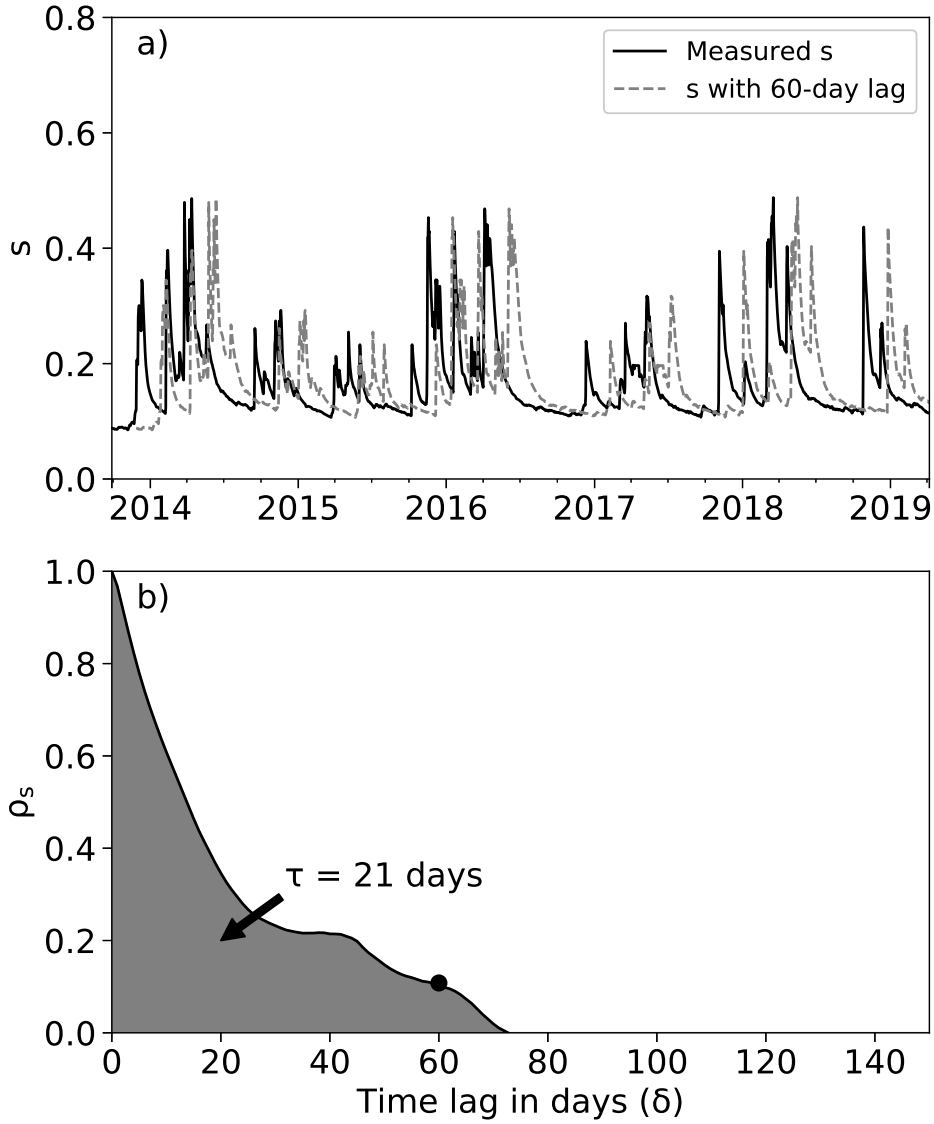

Figure 2: a) Example time series of depth averaged root-zone soil moisture and 60 days lagged time series of soil moisture. b) Corresponding autocorrelation function of the soil moisture time series. The memory timescale is the area under the autocorrelation function. The black dot indicates autocorrelation at 60-day lag.

When the spectra of $s(t)$ and its $TA(s)$ time series exhibit power-laws of the form $E_{ns}(f) \sim f^{-n}$ and $E_{TA}(f) \sim f^{-m}$, there exists an empirical relation between the spectral exponents given by

$$m = \frac{n+1}{2}\,, \tag{16}$$

where n is the spectral exponent of $s(t)$ and m is the spectral exponent of $TA(s)$. The relation is useful because the TA dynamics and the exponent m are analytically tractable for wide range of stochastic processes.

The dry period probability density function (PDF) is defined by the distribution of periods when $TA(s(t)) = 0$. The Self-Organized Criticality (SOC) predicts a PDF of the duration of dry periods and event sizes that exhibit power-laws of the form

$$\mathrm{PDF(T_d)} \propto T_d^{-\tau_d}, \quad \mathrm{PDF(M)} \propto M^{-\tau_s}\,, \tag{17}$$

where T_d is the dry period length, τ_d is the exponent of the dry period PDF, M is the event size and τ_s is the exponent of event size PDF. The event size is defined as the amount of water in continuous nonzero measurement of rainfall or fog deposition. For SOC systems near critical state, there exists a unique relation between the spectral exponent of the TA time series and the exponent of the dry period PDF given by

$$m = 3 - \tau_d\,, \tag{18}$$

which has been derived and confirmed for the avalanches of the classical sandpile model near critical slopes (Jensen, 1998).

The PDF of water-stress periods referred to also as dry persistence is the PDF of times when the value of soil moisture is below the water-stress point ($TA(s(t)) = 0$). These periods are forced by the interaction between precipitation distribution and the total loss term in the water balance equation. To compare dry persistence between the various measurement sites, the distribution of dry periods was normalized by the memory timescale and a stretched exponential function (Laherrère and Sornette, 1998) was fitted to the data. This function is given by

$$\mathrm{PDF(x)} = A_x x^{\beta-1} \exp\left(-x^{\beta}\right), \tag{19}$$

where $x = (I_{dry}/\tau)$ are the dry period length normalized by the memory time scale, $A_x = \beta \exp\left(x_{min}^{\beta}\right)$ is a normalizing constant needed to ensure that $\int_0^{\infty} \mathrm{PDF}(x)\, dx = 1$ and x_{min} is the shortest dry period. The fitting parameter β is assumed to be less

than unity. Smaller values of β indicate that long water-stress periods decay closer to power-law, whereas larger β indicates exponential decay at longer times. Commonly used least-squares fitting can produce inaccurate estimates of power law exponents (Clauset et al., 2009). Here, the Eq. 17 and 19 were fitted using a maximum-likelihood method, which identifies the portion of the distribution that follows the corresponding PDF function (Alstott et al., 2014).

The daily mean rainfall characteristics were calculated for complete rainfall time series for the soil moisture analysis across savannas and during early wet season for the carbon balance analysis at grazed savanna grassland. The daily mean precipitation depth (P_α mm event^{-1}) and daily mean storm frequency (P_λ events d^{-1}) are the parameters of the Poisson rainfall process (Rodriguez-Iturbe et al., 1999). The mean precipitation depth was calculated only for rainy days. This mean precipitation depth does not exactly correspond to the mean of event sizes M because these events may extend over two days. The mean storm frequency was calculated from the inverse of the mean time between rainy days.

2.5 Site descriptions

2.5.1 Grazed savanna grassland

The detailed analysis of carbon and water fluxes are presented from Welgegund grazed savanna grassland in South Africa from September 2010 to August 2016. The site is a private ranch located at 1400 m at the highveld area in South Africa. The annual mean rainfall at the site is 540 mm yr^{-1} with standard deviation of 112 mm yr^{-1} (**Paper II**). The plant species are typical savanna species with dominant tree species of *Vachellia erioloba*, *Searsia pyroides* and *Celtis africana*, and dominant grasses are *Eragrostis trichophora*, *Panicum maximum*, and *Setaria sphacelata*. The cattle grazing consists of about 1000 ± 300 heads of cattle for a 7000 ha area. This results in heavy grazing nearby around the footprint of the eddy covariance measurements. The tree cover is similar at the footprint from the main wind directions (**Paper II** supplement).

The woody and herbaceous LAI was sampled four times during one year. The total LAI ranged from 0.37 (July) to 2.32 m^{2}m^{-2} (April) (**Paper II**). The changes in vegetation state during the whole measurement period were quantified using the monthly average of MODIS 16-day Enhanced Vegetation Index (EVI) with 250 m spatial resolution

(MOD13Q1, collection 6) (Didan, 2015). To compare estimated T/ET to variations in vegetation phenology, the monthly average of MODIS 8-day LAI (MOD15A2H, collection 6) with 500 m spatial resolution was used to relate monthly T/ET to LAI. The EVI signal is a ratio of spectral bands, while the LAI has correct units of foliage area per ground area. The tree green-up dates were estimated from EVI signal by detecting the time when the EVI time series experiences a sudden increase ((Archibald and Scholes, 2007), **Paper I**). This increase was defined as the day when EVI signal was greater than a moving average of the previous four time steps.

2.5.2 African savannas

The analysis of measured root-zone soil moisture is presented for four African savannas with grass, grazed, tree, and miombo savanna vegetation (Fig. 3, **Paper III**). The grazed savanna is the same site from which the detailed carbon and water fluxes are presented. The measurements at the grass savanna site are located inside fenced meteorological station close to a maize farm in Kenya. This site has no influence of tree roots. The tree savanna measurements are located near Skukuza within Kruger National Park. The soil moisture measurements were taken from the Combretum apiculatum-dominated savanna. The tree canopy cover around the area is about 30 % (Archibald et al., 2009). The miombo savanna site is located within the Kataba Forest Reserve in Zambia (Kutsch et al., 2011). It is a woodland savanna characterized by a canopy cover of nearly 70 %. The soil moisture profile used in this study was located at the inter canopy space. Details of the measurement sites and instruments are presented in **Paper III**.

2.6 Fog measurements

The fog and rainfall measurements were made at an inland site in Kenya and at a coastal location in California. At the inland site, the meteorological and fog measurements were made from October 2013 to February 2016 at an opening within Vuria forest ($3°24'50''\text{S}, 38°17'29''\text{E}$) of the Taita hills. The site is surrounded by an upper montane cloud forest. At Taita hills, there are two rainy seasons with short rains from October to December and long rains from late March to June. The higher elevations receive more rain than lower elevations because of the orographic rainfall pattern, while

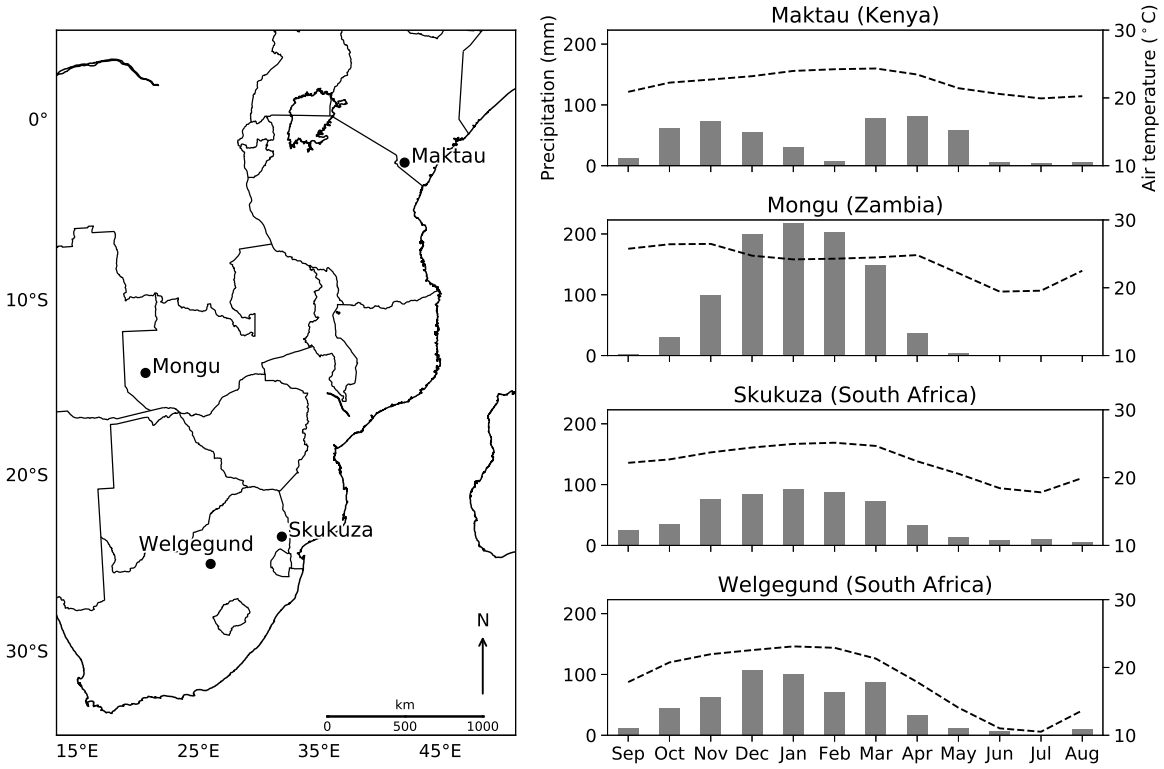

Figure 3: Location of the measurement sites: a grass savanna (Maktau, Kenya), a miombo savanna (Mongu, Zambia), a tree savanna (Skukuza, South Africa) and a grazed savanna (Welgegund, South Africa). The right panel shows the seasonal pattern of mean monthly rainfall and monthly air temperature at the sites.

the northwestern slope in the rain-shadow receives less precipitation than the south-eastern slopes (Pellikka et al., 2013). Seasonality and amount of rainfall vary over short distances depending on the altitude and the aspect of the slope, although the interannual variation of rainfall has strong spatial coherence (Nicholson, 2017). Due to the high-altitude location, the site has frequently advection fog, but radiation fog events are also possible. The fog and rainfall were sampled every minute and recorded every hour. The fog collector was a typical planar fog net with a double layer of Raschel-type netting (Schemenauer and Cereceda, 1994). The fog net surface area was 1 m^2 and the gutter area was 1.15 m by 0.12 m (= 0.138 m^2). The deposited fog water was measured using a tipping bucket rain gauge protected from rainfall. The fog net was facing northwest (320°) and southeast (140°) and had a metal plate roofing covering it from rainfall.

The coastal Northern Californian measurements were located above chaparral rangeland, on the San Francisco Peninsula, at 329 m above the sea level. The fog collector was a Juvik-type radial collector. Chung et al. (2017) describes the spatial analysis of fog at this watershed. The fog deposition and rainfall were measured from June 2014 to September 2016. The fog deposition was not measured during winter months at this site, but it is expected that non-rainfall-related fog events are minimal relative to rainfall during the winter months. The rainfall was continuously measured except during one 40-day-long gap in November 2015.

The fog deposition during rainfall was excluded from the analysis, and fog events that had rainfall events of 1.0 mm or larger two hours before the fog event were excluded from the fog record. Both rainfall and fog events were defined as a continuous nonzero measurement of rainfall and fog. Isolated 0.2-mm/h events were also removed from both time series as this is the detection limit of the tipping bucket.

3 Results and discussion

3.1 Precipitation and transpiration at grazed savanna grassland

The annual precipitation varied from 421 to 614 mm yr^{-1} at the grazed savanna grassland in South Africa (Table 1). The hydrological years 2010, 2012, 2013 and 2014 were years with close to or above the long-term mean annual precipitation of 540 mm yr^{-1}. The measured annual ET was similar to or greater than the measured annual precipitation. In 2011 the measured annual precipitation was 187 mm lower than the measured annual ET. The year 2015 was a drought year with infrequent rainfall lasting 11 months. The P–ET was not related to the surface soil moisture storage changes but inversely related to the maximum EVI (Fig. 4).

Gapfilling of the nighttime evapotranspiration (ET_N) and wind-induced underestimation of rainfall measurements, are likely reasons for the mismatch in the annual water balance. Due to frequent afternoon and nighttime precipitation, the nighttime evapotranspiration was 12 % of the annual ET (Table 1). The annual P–ET would be positive for four years (2012–2015) if ET_N was assumed to be zero. The gapfilled ET_N might be an overestimate because only 30 % of the values were measured and these values were determined during high wind conditions ($u^* > 0.28$ m s^{-1}). A comprehensive study estimated the underestimation for the rain gauge (Casella) at 0.5 m height to be 9.4 % at the measurement site with similar mean wind speed (5 m s^{-1}) and annual rainfall (P=700–1000 mm yr^{-1}) (Pollock et al., 2018). At higher wind site, the underestimation was 11 % at 0.5 m height and 17 % at 1.5 m height. The 9.4 % underestimation can be considered a minimum, and annual P adjustment (i.e. 1.094 measured P) would lead to annual mean P $\approx$ ET for five years, excluding the year 2011. The possibly higher underestimation of rainfall in 2011 could be due to larger spilling error due to higher rainfall intensity evidenced by the shortest total duration of rainfall in 2011. In addition, the single soil moisture profile measurement that is far from the trees does not represent well the soil water storage change of the footprint area that includes both the lateral and deep roots of the trees. The surface runoff is small because the site is located at a flat thornveld. The possibility of overestimating annual ET due to advection from surrounding ranch or maize field was also tested by excluding ET from the northwest or south directions. However, the annual P–ET was

increased less than 11 mm each year after excluding either of the two wind directions. Therefore, the most likely reasons for the annual residual is the underestimation of annual rainfall and the overestimation of nighttime evapotranspiration.

The high ET/P ratios at this site agree with the study in Nylsvley, South Africa, where it was estimated that the long-term average deep drainage is 1 % of annual precipitation, and it occurs rarely during the abnormally wet years (Scholes and Walker, H., 1993). Savannas without significant tree cover have had lower ET/P ratios. For example a millet field in Niger, the ET/P ranged from 82 to 85 % (P=500 $\mathrm{mm\,yr^{-1}}$) (Velluet et al., 2014) and the ET/P was 80 % at semi-arid shrubland in Kenya (P=674 $\mathrm{mm\,yr^{-1}}$) (Odongo et al., 2016).

During the wet years (2010 and 2012–2014), the estimated annual transpiration was highly constrained to $352 \pm 8\ \mathrm{mm\,yr^{-1}}$ (T/ET=0.55), and the cumulative transpiration was similar. In contrast, the year 2011 and the drought year 2015 had lower transpiration from early wet season onwards (Fig. 4). The difference between the lowest and the highest annual T/ET during the wet years was less than 0.09 (Table 1), which is an upper limit for a given ecosystem from a joint modeling and observation analysis (Paschalis et al., 2018). However, during the drought year, the annual T/ET was reduced substantially to 0.39 due to grass dieback-regrowth and possibly due to other changes in soil surface properties that enhanced evaporation (**Paper I**).

The comparison of year 2013 and 2012 showed that in year 2013 the higher precipitation frequency resulted in larger monthly T/ET during the rainy season (Fig. 5, **Paper I**). These two years can be compared due to similar carbon balance and NDVI trend that represents LAI changes (Fig. 7, **Paper I**). The tree green-up was earliest in year 2011 that resulted in high T/ET at the start of the rainy season (Fig. 5).

In summary, the annual precipitation was highly variable in amount and in timing. However, the annual transpiration and T/ET were nearly constant and reduced only during the severe drought year. The monthly course of T/ET is complicated due to the early green-up of trees and due to grass growth that is coupled to the precipitation variability. Further analysis of the T/ET could be done using dual source model of ET that separates soil and vegetation components (Shuttleworth and Wallace, 1985; Li et al., 2019).

Table 1: Annual sum of water balance components for each hydrological year (September to August). The annual P at the measurement site is followed by the annual P at the SAWS Potchefstroom station in parentheses for comparison (**Paper I**). The total uncertainty is indicated for ET after ± sign. ET_N is the annual nighttime evapotranspiration. The transpiration and evaporation are calculated from monthly T/ET estimates. $\Delta\Theta_{1m}$ is the annual change in stored soil water for 0–1 m soil layer. The residual is $P - ET - \Delta\Theta_{1m}$. P_d is the total duration of rainfall during each year. The EBC-slope stands for the slope of the energy balance closure with ordinate defined by measured Rn–G and abssisa defined by the sum of the measured latent and sensible heat fluxes.

Year	P (mm/yr)	ET[a] (mm/yr)	ET_N (mm/yr)	P–ET (mm/yr)	T (mm/yr)	E (mm/yr)	$\Delta\Theta_{1m}$ (mm/yr)	Residual (mm/yr)	T/ET	PET (mm/yr)	EVI_{max}	P_d (hours)	EBC-slope	Green-up (DOY)
2010–2011	574 (332)	658 ± 8	68	–84	362	295	-	–84	0.55	1133	0.32	266	0.75	238
2011–2012	421 (560)	608 ± 10	68	–187	291	317	-	–187	0.48	1123	0.30	121	0.80	230
2012–2013	614 (537)	667 ± 8	78	–53	352	314	14	–67	0.53	1109	0.29	159	0.85	242
2013–2014	530 (509)	600 ± 6	81	–70	348	252	12	–82	0.58	1039	0.31	153	0.81	254
2014–2015	582 (407)	642 ± 11	85	–60	344	297	3	–63	0.54	1057	0.27	158	0.83	241
2015–2016	465 (437)	463 ± 6	58	2	179	283	–1	3	0.39	1038	0.22	157	0.84	241
Mean	531	606	73	–75	313	293	5	-80	0.51	1083	0.28	169	0.81	241
SD	68	69	10	57	64	22	6	61	0.06	40	0.03	45	0.03	7

[a]The total uncertainty is calculated as $E_{rand,k} = \sqrt{\sum_{i=1}^{n} \sigma_i^2}$ for year k. The square root was missing in the Eq. 3 in **Paper III**.

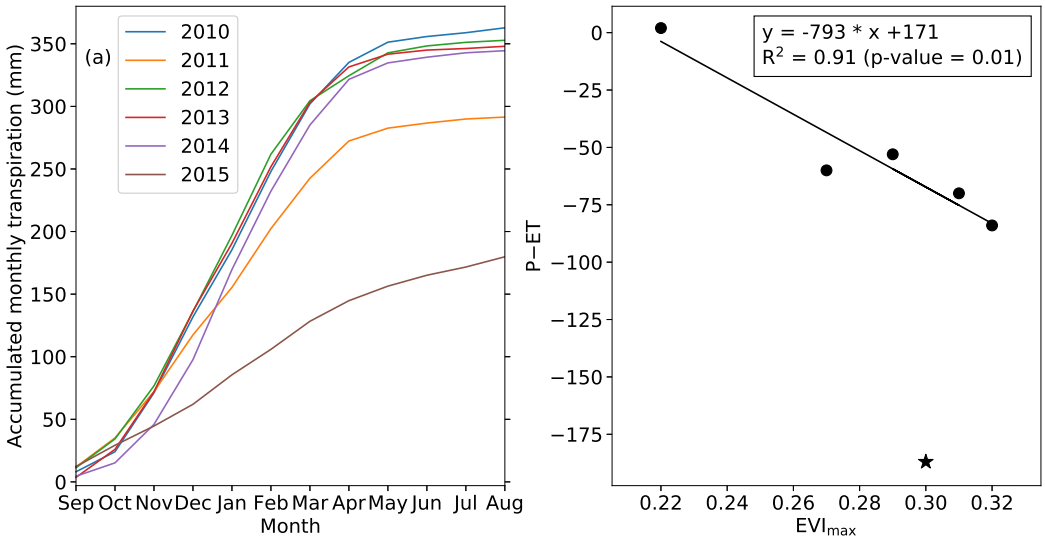

Figure 4: a) Cumulative monthly transpiration for each hydrological year (September to August). b) Relationship between annual maximum EVI and P–ET. The year 2011 (star) is not considered in the fit due to uncertain precipitation. Adopted from **Paper I**.

3.2 Annual carbon balance of grazed savanna grassland

The Welgegund savanna grassland was a carbon source during five out of six measured years. The annual NEE ranged from –58 to 198 $\mathrm{gC\,m^{-2}\,yr^{-1}}$ with six-year mean of 98 $\mathrm{gC\,m^{-2}\,yr^{-1}}$ (Table 2). The high respiration is likely due to the cattle respiration and the flux from the dung decomposition that increase the total ecosystem respiration. Their magnitude could not be estimated because the grazing area is much larger than the eddy covariance footprint area. The annual NEE calculation is also affected by the calculation of storage flux. In the **Paper II** the two-point estimated storage flux resulted in 51 $\mathrm{gC\,m^{-2}\,yr^{-1}}$ less than the NEE based on a single CO_2 concentration measurement level. The annual NEE range at Welgegund site is similar to the annual NEE measured at Skukuza, South Africa (30 % tree cover) where two of the five years had negative NEE (Archibald et al., 2009). Potential drivers of interannual variation for carbon fluxes are presented in Figure 6. The annual NEE was related to annual maximum NDVI, and it was lower for higher annual PET. The NDVI value is a mixture of tree and grass components, but the variance of annual maximum is most likely related to the maximum grass leaf area. The annual cumulative GPP was also related

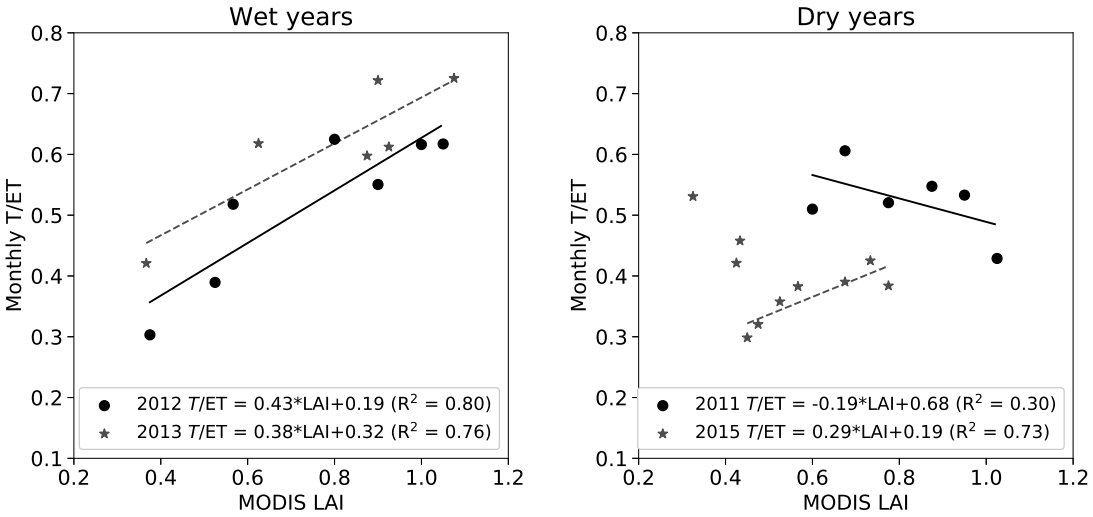

Figure 5: Rainy season relation between monthly MODIS LAI and T/ET for wet (2012 and 2013) and dry (2011 and 2015) years. The year 2013 had higher early wet season precipitation than year 2012. In 2015 the November, May, and June values were excluded as outliers from the fit. Adopted from **Paper I**.

to maximum NDVI. The annual respiration was strongly correlated with the amount of rainfall in the early wet season. The rainy season length or early season precipitation frequency were not related to any of the annual carbon fluxes, and the annual NEE was related to the wet soil days only during the first three years (**Paper II**). The drought year had above mean number of wet soil days distributed along 11 months, and thus the number of wet soil days does not necessarily relate to plant available water.

The cumulative NEE has a different trend during each year (Fig 7). The early wet season NEE was positive and increasing except in 2011 when it was near zero. This might be explained by the earliest tree green-up compared with other years that resulted in high early season tree transpiration and high T/ET during this period. The P–ET was also the lowest in 2011 and might be partly explained by higher deep-water uptake of the *Vachellia erioloba* trees. These specific trees were shown to take 37 % of their water from below 1 m depth in the end of dry season (Beyer et al., 2018). The year 2010, with the highest peak NDVI and high frequency of early season rainfall, resulted in high carbon uptake. However, in 2013 the frequent early season rainfall did not lead to high carbon uptake during the mid-rainy season (Table 2). In the drought year 2015, the cumulative NEE was decreasing only during the dry season (June-August).

There was an unusual 60 mm rain event in July (Fig. 1, **Paper I**), during which there was no active grass layer and thus the trees uptake carbon. This increase in tree photosynthesis is also confirmed by the cumulative increase in dry season transpiration in 2015 compared to other years (Fig. 4).

The year 2011 shows that at this site the reduction of rainfall frequency does not necessarily lead to a reduction in carbon assimilation due to early greening of trees that is decoupled from the rainfall. Manipulation experiment with C_4 grassland has shown that decreasing precipitation frequency reduces carbon assimilation (Knapp et al., 2002). However, irrigation experiment with savanna trees at the end of dry seasons shows that surface soil moisture state may not trigger the early greening (Whitecross et al., 2016). Increasing temperature might potentially drive the early greening (Campo-Bescós et al., 2013; Whitecross et al., 2017), but the NDVI derived green-up dates (**Paper I**) were not related to mean or maximum air temperature in August. The daily mean rainfall statistics were also calculated during the complete rainy season periods defined in **Paper I**, but these did not explain the variance in annual carbon fluxes. A more detailed analysis of the effect of rainfall frequency on carbon balance is not possible due to high variability in the annual rainfall amounts.

The results show that the interannual variance of NEE is high and it was related to annual maximum NDVI and PET. Interestingly, there is strong correlation between early season rainfall and annual respiration. The contribution of deep-rooted trees for carbon balance is confirmed by the high carbon uptake during anomalous dry season precipitation and after the earliest green-up of trees. The wet soil days or precipitation frequency did not explain the annual fluxes. Therefore, the aggregated measures of actual grass and tree water uptake are needed to better understand the variance in NEE.

Table 2: Annual carbon balance and key environmental drivers calculated for each year from September to August of the following year. The wet soil days are defined as days when soil moisture at 5 cm depth was greater than 7 %. The P_α is the daily mean precipitation depth, and P_λ is the daily mean storm frequency calculated for early wet season.

Year	NEE ($\mathrm{gC\,m^{-2}\,yr^{-1}}$)	GPP ($\mathrm{gC\,m^{-2}\,yr^{-1}}$)	Respiration ($\mathrm{gC\,m^{-2}\,yr^{-1}}$)	Peak NDVI	P (Sep-Dec) ($\mathrm{mm\ (4\,months)^{-1}}$)	Total wet soil days (days)	P_α (Sep-Dec) ($\mathrm{mm\,event^{-1}}$)	P_λ (Sep-Dec) ($\mathrm{events\,d^{-1}}$)
2010–2011	–58 ± 31	–1061	1003	0.57	273	224	5.0	0.44
2011–2012	69 ± 23	–811	881	0.50	175	100	6.6	0.21
2012–2013	129 ± 22	–921	1051	0.49	311	73	6.1	0.35
2013–2014	138 ± 65	–884	1023	0.51	272	72	6.8	0.47
2014–2015	111 ± 25	–772	884	0.49	192	157	6.4	0.38
2015–2016	198 ± 22	–562	761	0.40	142	163	5.9	0.14
Mean	98	–835	934	0.49	228	132	6.1	0.33
SD	79	153	101	0.05	61	55	0.6	0.13

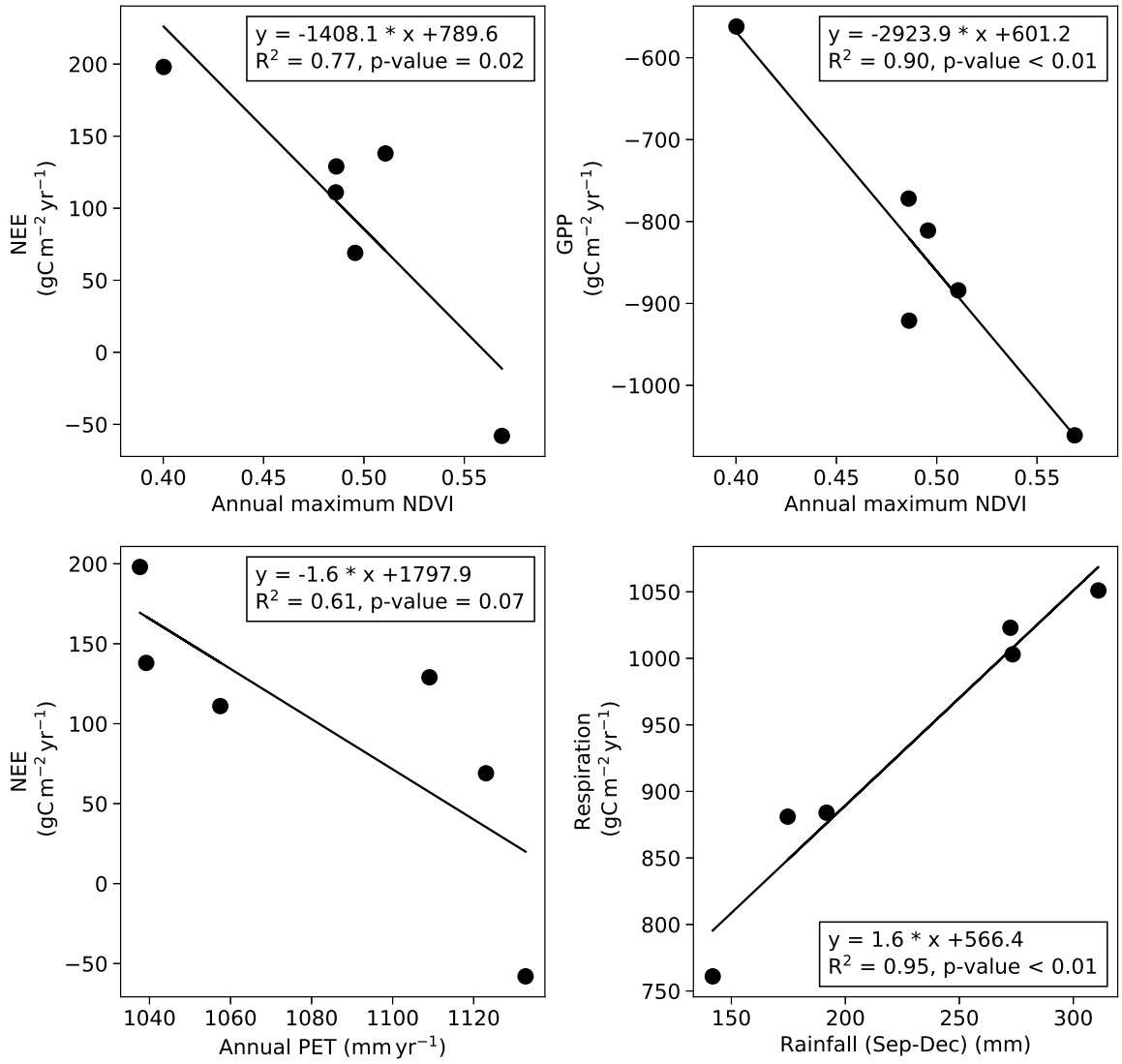

Figure 6: Annual NEE, GPP, and respiration compared with potential drivers of inter-annual variability: annual maximum NDVI, annual PET, and early season rainfall.

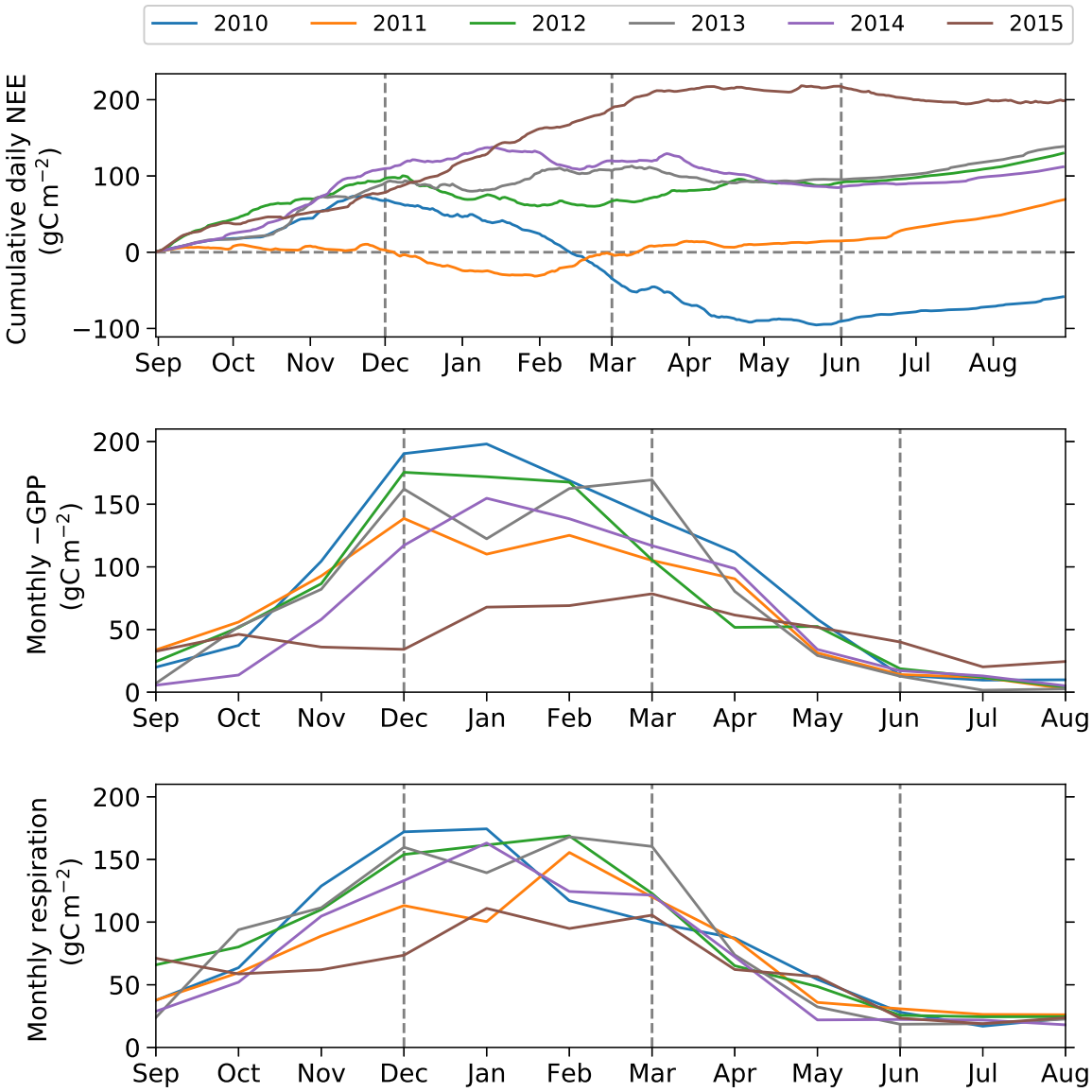

Figure 7: Cumulative daily NEE, monthly GPP, and respiration for each hydrological year (September to August).

3.3 Soil moisture variability across African savannas

The mean root-zone soil moisture variability across four African savannas was analyzed using a hierarchy of water balance models (Eqs. 8, 9, 10). The jumps in measured soil moisture largely match in timing jumps in modeled soil moisture at all sites (Fig. 8). The measured precipitation was reduced by the constant γ that represents interception, re-evaporation and any spatial mismatch between rainfall and soil moisture. The relation between cumulative soil moisture increase and cumulative precipitation was non-linear at the beginning of the wet season at the tree and miombo savanna (**Paper III**). At the grazed savanna site, this relation deviated from the assumed linear relation between November 2013 and November 2014, which resulted in an underestimation of modeled soil moisture during this period (Fig. 8). The soil moisture decay rates of models 2 and 3 (with NDVI and NDVI-PET adjustments to E_{max}) are comparable to the measured soil moisture decay. Model 1, with constant maximum evapotranspiration, overestimates the soil moisture decay, especially during the transitions from dry to wet and wet to dry periods. The comparison of spectral exponents of soil moisture between different models showed that the model 1 with rainfall variability captured a large part of soil moisture spectral decay and the NDVI (model 2) and PET (model 3) did not add energy to the seasonal time scales in soil moisture spectrum (**Paper III**). However, the NDVI and NDVI-PET adjustments were necessary for correct soil moisture memory (Eq. 13) and estimation of the β parameter for dry period distribution (Eq. 19, **Paper III**).

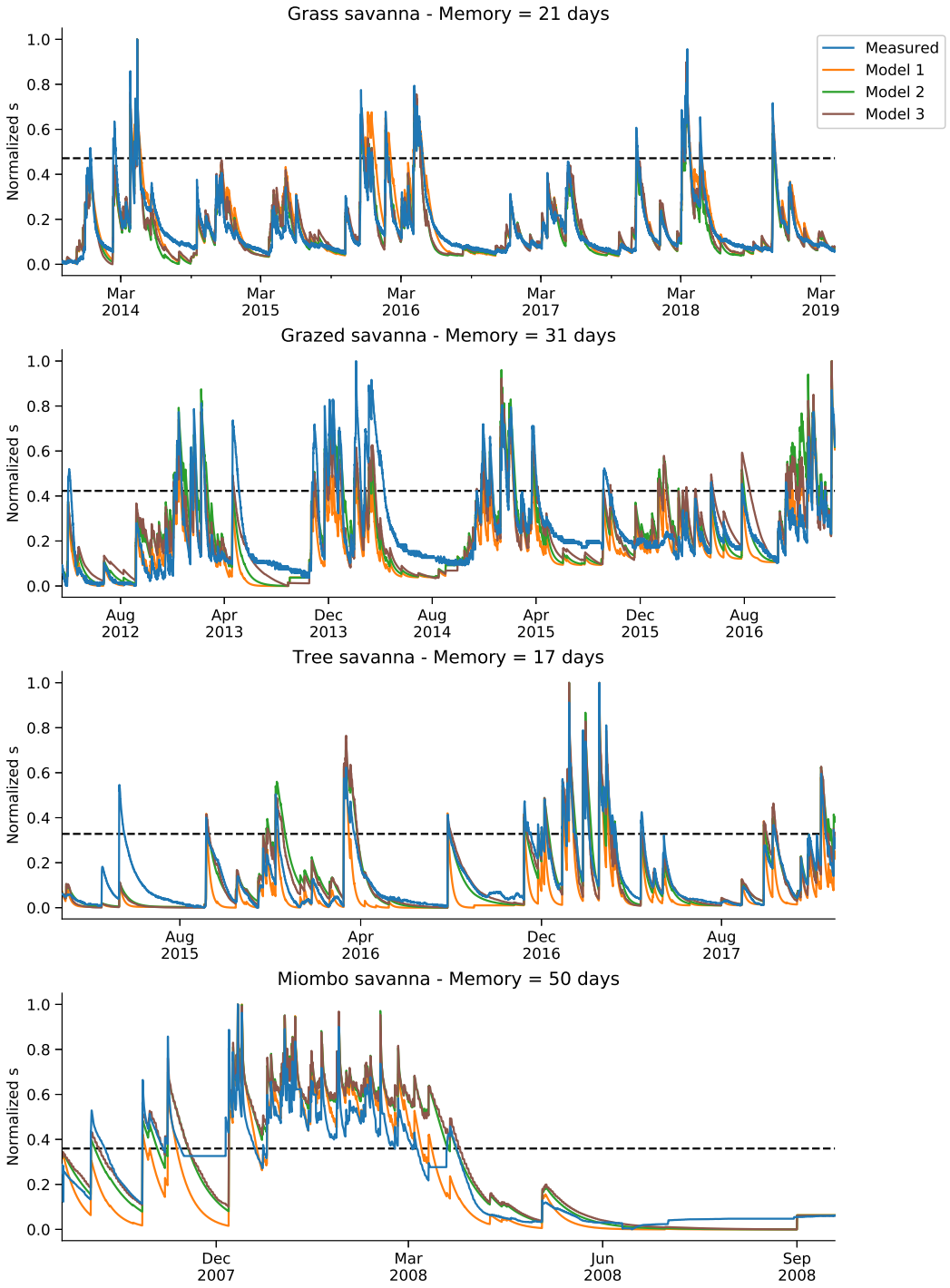

Figure 8: Time series of normalized soil moisture. The soil moisture values were rescaled to zero to one range. The dashed line indicates the normalized value of the water stress point (s^*). The memory timescale of the measured soil moisture series is indicated for each site. Adopted from **Paper III**.

The measured soil moisture memory timescale varied from 17 to 50 days (Fig. 8). The daily mean rainfall intensity and measured memory timescale were linearly related across three savannas where ET is comparable to infiltration (ET/infiltration $\approx$ 1.0) (Fig. 9). This means that there is a link between rainfall statistics and maximum ET. When ET/infiltration $\approx$ 1.0, then the losses are dominated by ET at long time scales and they equal the mean rainfall intensity adjusted by interception loss (Eq. 2.46, Rodríguez-Iturbe and Porporato (2007)). This relationship was also shown at the three sites with stochastic Poisson precipitation that includes dry seasons using the model 2 with NDVI variability on maximum evapotranspiration (Fig. 8, **Paper III**). This relationship could be used to explore how precipitation seasonality affects soil moisture variability without separating the analysis between dry and wet seasons. The intensity-memory relationship might be different at sites with highly seasonal precipitation because long dry periods decrease precipitation intensity, and drainage might become a much more significant contributor to the loss term in the hydrological balance.

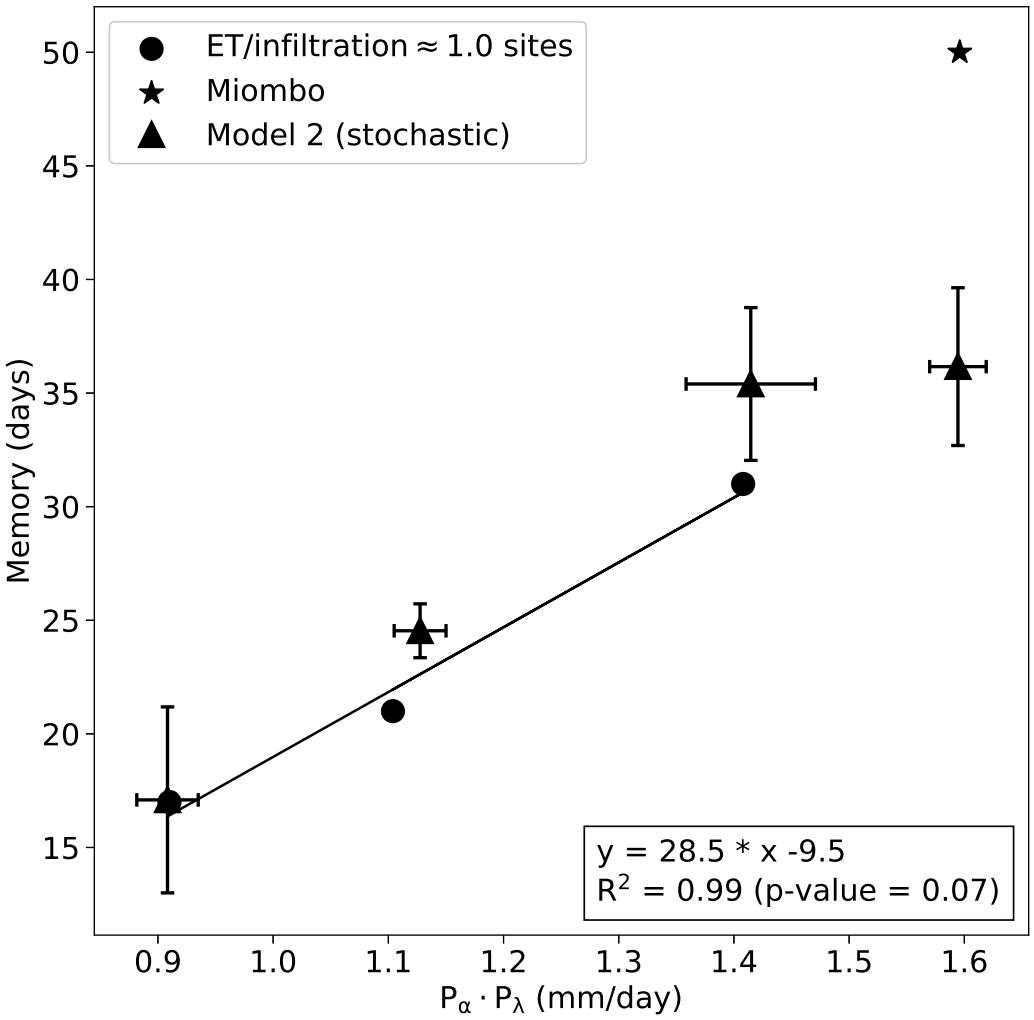

Figure 9: The relationship between daily mean rainfall intensity, $P_\alpha \cdot P_\lambda$, and the soil moisture memory timescale. The dots indicate measured values for the three sites with ET/infiltration $\approx$ 1.0, and the star indicates the measured value at miombo. The triangles indicate mean values, and error bars indicate ± 1 standard deviation from 50 stochastic simulations. Adopted from **Paper III**.

The distribution of times when soil moisture was below the plant water-stress threshold revealed that the savannas can either have closer to power-law or exponential decay at long times. Model 3 was able to distinguish the smaller β values that indicate power-law scaling and larger β values that indicate exponential decay (Fig. 10). At Kenyan grass savanna, the timing and length of the dry period between the short and long rainy seasons are highly variable. Also, during the long rains, there can be significant in-season dry spells. Further analysis of the structure of precipitation variability in East Africa and its implications for rainfed farming are important future research topics to be analyzed in the stochastic ecohydrological framework.

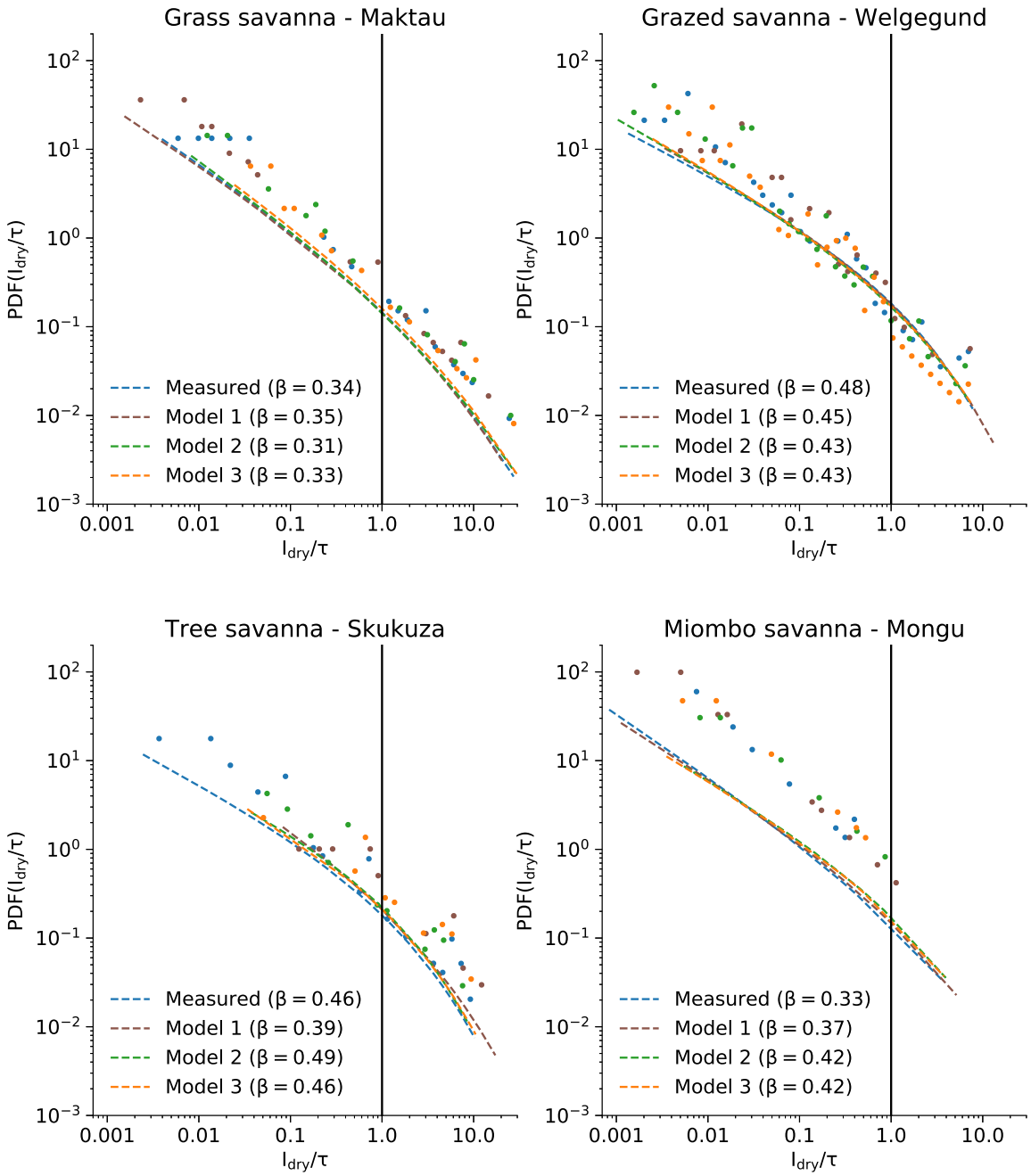

Figure 10: The probability density function (PDF) of persistence times of soil moisture below s^* divided by the site-specific memory timescale. The blue, brown, green, and yellow lines indicate the fit to the Eq. 19 for the measured, Model 1, Model 2 and Model 3 results. The dots indicate logarithmically spaced bins. The vertical lines indicate the memory timescales determined at 21, 31, 17 and 50 days for the grass, grazed, tree, and miombo savannas. Adopted from **Paper III**.

3.4 Similarity in fog and rainfall intermittency

The connection between precipitation and fog at inland tropical cloud forest and coastal rangeland in Northern California was analyzed to understand whether fog deposition has a similar statistical structure as rainfall.

The rainfall and fog deposition spectra showed a power-law decay at subdaily periods (Fig. 11). The spectra of the on-off time series (TA series, Eq. 14) were similar. The fog spectrum at the coastal site had a flattening at the high frequency that is likely due to inadequate sampling. The spectral decay of the TA series showed that similar scaling is evident in rainfall and fog at both sites (TA exponents from $m \approx 0.76 - 0.95$), and this scaling extends from hour to monthly timescales. These TA exponents are close to the previously reported value of 0.84 derived from five sites with different rainfall formation patterns (Molini et al., 2009).

The dry period and event size PDF of rainfall and fog deposition show power-law scaling (Fig. 12). The scaling exponents of the dry period PDFs were 1.33 and 1.41 for fog and 1.44 and 1.40 for rainfall at the coastal and inland sites, respectively. These rainfall exponents are similar to the ones reported in Germany (Peters and Christensen, 2006) and on the Mediterranean coast in Spain (Deluca and Corral, 2014).

The switching between on and off states of rainfall and fog was not entirely independent of the amplitude intermittency due to deviations from the relation in Eq. 18. The differences between the prediction of TA exponents from Eq. 18 and the measured TA exponents were -0.61 to -0.84 (**Paper IV**). This means that the amplitude variations impact the relation between the TA exponent (m) and the exponent of the dry period PDF (τ_d), and the SOC model cannot fully explain all the aspects of the on-off and off-on switching for fog and rainfall despite the power-laws in statistics evaluated here. In turbulence studies, this deviation has been attributed to the intermittency corrections, μ_I, ($m + \tau_d = 3 - \mu_I$) but here the intermittency corrections estimated using second-order gradients were insufficient in all cases (**Paper IV**).

This analysis showed analogies between rainfall and fog deposition based on the SOC paradigm. The satellite detection of fog could be combined with the presented analysis methods to delineate the primary controls of fog frequency over a broad range of timescales. Satellite fog detection algorithms have been used in California's Central Valley and mountainous locations in Taiwan (Baldocchi and Waller, 2014; Schulz et al., 2016). These kinds of data sets may allow to extend the presented analysis in order to understand environmental control parameters of fog over a broad range of timescales.

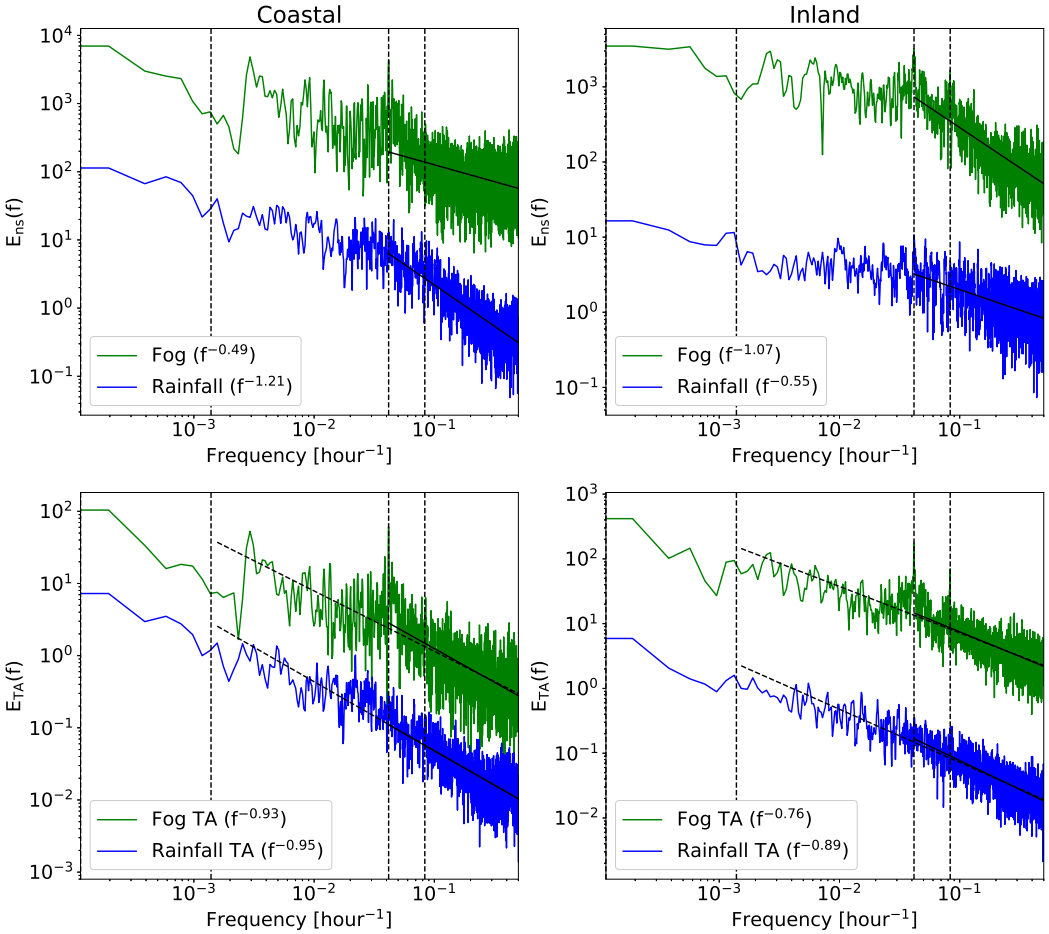

Figure 11: Normalized spectrum of fog and rainfall time series and their corresponding telegraphic approximation (TA) spectra. The linear fit is up to 1 day, and the dashed fit line extends to 1 month. The dashed vertical lines show frequencies corresponding to 12-hr, 24-hr, and 1-month timescales for clarity. The fog spectra were shifted along the y-axis to permit comparisons. Adopted from **Paper IV**.

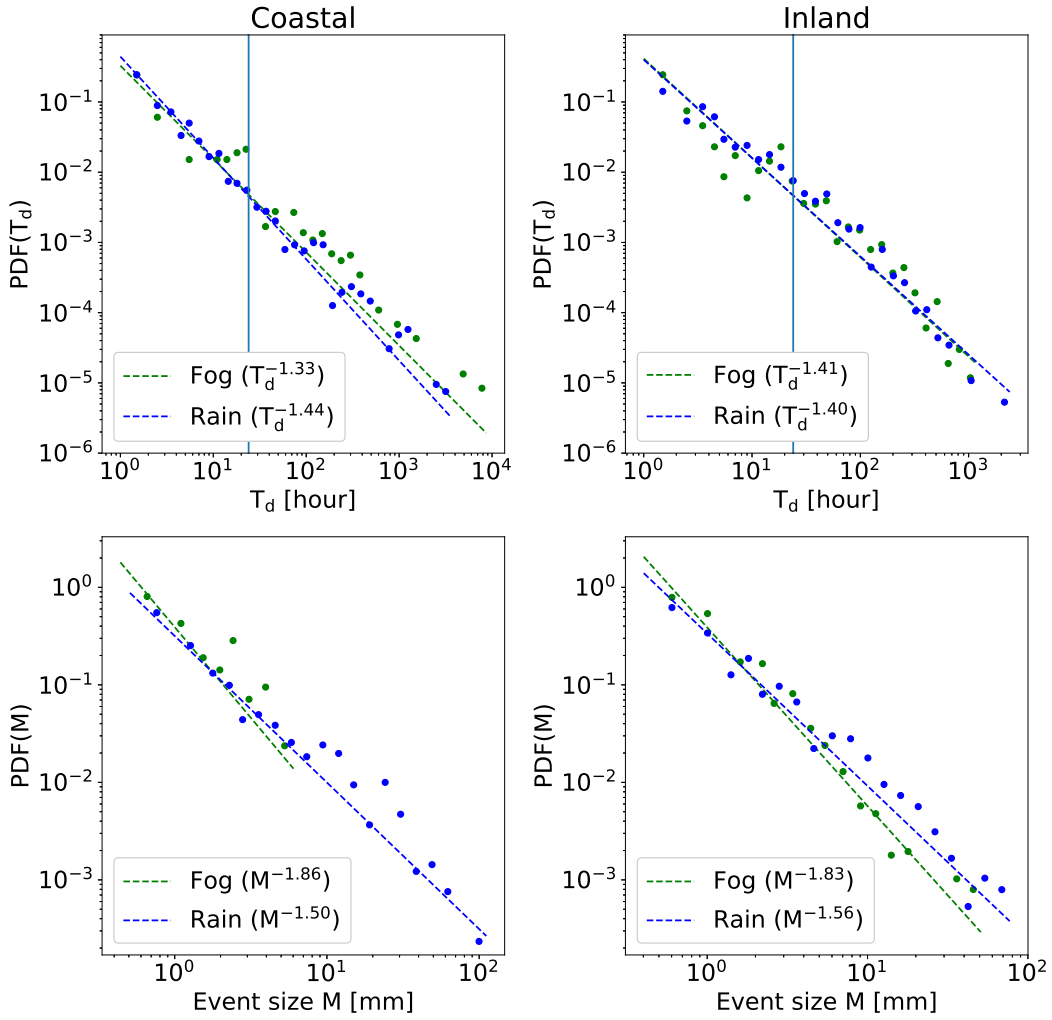

Figure 12: The probability density functions (PDFs) of the duration of dry periods and the event sizes for rainfall and fog deposition measurements (Eq. 17). The blue vertical line denotes a 1-day period. Note that the rainfall and fog deposition size PDFs do not have the same units because the fog deposition amount has units of millimeters per 1 m^2 of fog net. Adopted from **Paper IV**.

4 Conclusions

This thesis has presented long-term carbon and water balances of a grazed savanna grassland in South Africa and soil moisture variability across four African savannas. In addition, the similarities in the on-off switching of rainfall and fog were compared at inland and coastal sites.

The main conclusions are as follows:

(1) The annual precipitation was highly variable in amount and timing at the grazed savanna grassland. However, the estimated annual transpiration, which was based on annually fitted water use efficiency and optimality hypothesis, was nearly constant during wet years and reduced during drought year with intermittent rainfall. The reduction in transpiration was due to grass dieback-regrowth and possibly due to other changes in soil surface properties that enhanced evaporation. The monthly course of the T/ET ratio varied due to the early green-up of trees and due to grass growth that is coupled to the precipitation variability.

(2) The annual NEE ranged from –58 (sink) to 198 (source) $\mathrm{gC\,m^{-2}\,yr^{-1}}$ at the grazed savanna grassland. The interannual variation in NEE and GPP was related to peak NDVI, and the annual respiration was strongly correlated with early season rainfall amount. The contribution of deep-rooted trees (*Vachellia erioloba*) to the carbon balance was shown by the carbon uptake during anomalous dry season precipitation and after early green-up of trees in 2011. In 2010, the early season rainfall was frequent and annual carbon balance was negative, whereas, in 2013, the frequent early rainfall did not result in high carbon uptake during the subsequent wet season. Separate tree and grass leaf phenology and water uptake patterns are needed to explain the variance in NEE in these ecosystems.

(3) The analysis of root-zone mean soil moisture showed that soil moisture variability is largely explained by rainfall variability. However, the water balance model with constant maximum evapotranspiration resulted in the overestimation of the soil moisture decay. The NDVI and PET adjustment to ET losses improved the model fit by accounting for interannual variation in ET. The soil moisture memory timescale, a rough measure of the time it takes for a soil column to forget the initial soil moisture state, was linearly related to daily mean precipitation intensity at sites where ET was comparable to infiltration. This means that there is a link between rainfall statistics

and maximum ET, even though the memory timescale is primarily controlled by ET and drainage losses.

(4) The analysis of fog and rainfall series showed that fog intermittency has certain similarities that have been documented for rainfall in earlier studies. The on-off series for fog and rainfall exhibited an extensive power-law scaling beyond the timescales of the spectra of the original series with exponent $m \approx 0.8$. These exponent values agree with previous studies on rainfall time series. The dry period and event size PDF of rainfall and fog deposition showed a power-law scaling. This allowed to suggest the analogy with Self-Organized Criticality, which relates the m exponent and dry period exponent (τ_d). However, this relation did not hold for rainfall and fog, and the intermittency corrections did not recover this relation. Therefore, the on-off switching was not entirely independent of the amplitude intermittency in fog and rainfall. Satellite detection of fog may allow further analysis of these properties of fog over broader spatial and temporal scales, which could be used to characterize the role of fog for cloud forests.

The analysis of ecosystem-scale fluxes revealed that annual changes in vegetation dynamics can affect the carbon and water balance of savannas with significant tree cover. The dry season activity of trees resulted in higher carbon uptake shown by the early green-up of trees and increased tree photosynthesis after dry season rainfall event. The tree green-up was inferred from NDVI, and the annual NDVI was linked to the ecosystem productivity. The analysis of continuous precipitation and soil moisture time series revealed an interesting emergent relationship between precipitation intensity and soil moisture memory timescale. These observations suggest that the use of measured rainfall intermittency and phenology derived from NDVI could be used as forcing for a minimalist carbon and water balance model. The model could be used to delineate the primary mechanisms of legacy effects in carbon and water balance between years, which may help to interpret further the interannual variation in the ecosystem-scale fluxes.

5 Review of papers

Paper I: The main aim of this study was to estimate annual and monthly transpiration from evapotranspiration measurements at a grazed savanna grassland. The estimated annual transpiration was nearly constant during wet years but was reduced during a severe drought year. The developed ET partitioning methodology can be used in a range of arid and semi-arid ecosystems.

Paper II: This study reported measurements of carbon dioxide exchange from a grazed savanna grassland ecosystem for three years. The night-time respiration was not dependent on soil moisture or soil temperature on weekly timescales. The annual variation of carbon balance was related to changes in early wet season and mid-growing season fluxes.

Paper III: The main aim of this study was to interpret the temporal variability in the root-zone soil moisture at four African savannas across a rainfall gradient. The hierarchy of ecohydrological models showed that precipitation variability explains a large part of the soil moisture variability. However, the comparison of model memory estimates shows that to model the soil moisture variability correctly, the constant daily maximum ET has to be adjusted with NDVI and PET. At semi-arid savannas, the mean precipitation intensity and memory timescale were linearly related.

Paper IV: The main aim of this study was to compare fog and rainfall statistics at an inland cloud forest and coastal forest. The results showed that the spectral exponents of the on-off time series of fog and rainfall are similar and correspond to previous estimates from different rainfall regions. This shows that fog intermittency is similar to rainfall, which suggests that the stochastic models of rainfall intermittency could also be used to estimate fog occurrence.

References

Ago, E. E., Agbossou, E. K., Galle, S., Cohard, J.-M., Heinesch, B., and Aubinet, M. (2014). Long term observations of carbon dioxide exchange over cultivated savanna under a Sudanian climate in Benin (West Africa). *Agricultural and Forest Meteorology*, 197:13–25.

Al-Kaisi, M., Brun, L. J., and Enz, J. W. (1989). Transpiration and evapotranspiration from maize as related to leaf area index. *Agricultural and Forest Meteorology*, 48(1):111–116.

Alstott, J., Bullmore, E., and Plenz, D. (2014). Powerlaw: A Python package for analysis of heavy-tailed distributions. *PLOS One*, 9(1).

Archibald, S. and Scholes, R. J. (2007). Leaf green-up in a semi-arid African savanna – separating tree and grass responses to environmental cues. *Journal of Vegetation Science*, 18(4):583–594.

Archibald, S. A., Kirton, A., van der Merwe, M. R., Scholes, R. J., Williams, C. A., and Hanan, N. (2009). Drivers of inter-annual variability in Net Ecosystem Exchange in a semi-arid savanna ecosystem, South Africa. *Biogeosciences*, 6(2):251–266.

Aubinet, M., Vesala, T., and Papale, D. (2012). *Eddy covariance*. Springer Netherlands, Dordrecht.

Baldocchi, D. and Waller, E. (2014). Winter fog is decreasing in the fruit growing region of the Central Valley of California. *Geophysical Research Letters*, 41(9):3251–3256.

Berkelhammer, M., Noone, D. C., Wong, T. E., Burns, S. P., Knowles, J. F., Kaushik, A., Blanken, P. D., and Williams, M. W. (2016). Convergent approaches to determine an ecosystem's transpiration fraction. *Global Biogeochemical Cycles*, 30(6):933–951.

Beyer, M., Hamutoko, J. T., Wanke, H., Gaj, M., and Koeniger, P. (2018). Examination of deep root water uptake using anomalies of soil water stable isotopes, depth-controlled isotopic labeling and mixing models. *Journal of Hydrology*, 566:122–136.

Bond, W. J. (2008). What limits trees in C_4 grasslands and savannas? *Annual Review of Ecology, Evolution, and Systematics*, 39(1):641–659.

Bruijnzeel, L. A., Eugster, W., and Burkard, R. (2005). Fog as a hydrologic input. In Anderson, M. G. and McDonnell, J. J., editors, *Encyclopedia of Hydrological Sciences*. John Wiley & Sons, Ltd, Chichester, UK.

Brümmer, C., Falk, U., Papen, H., Szarzynski, J., Wassmann, R., and Brüggemann, N. (2008). Diurnal, seasonal, and interannual variation in carbon dioxide and energy exchange in shrub savanna in Burkina Faso (West Africa). *Journal of Geophysical Research: Biogeosciences*, 113.

Campo-Bescós, M. A., Muñoz-Carpena, R., Kaplan, D. A., Southworth, J., Zhu, L., and Waylen, P. R. (2013). Beyond precipitation: Physiographic gradients dictate the relative importance of environmental drivers on savanna vegetation. *PLOS One*, 8(8).

Chung, M., Dufour, A., Pluche, R., and Thompson, S. (2017). How much does dry-season fog matter? Quantifying fog contributions to water balance in a coastal California watershed. *Hydrological Processes*, 31(22):3948–3961.

Clauset, A., Shalizi, C. R., and Newman, M. E. J. (2009). Power-law distributions in empirical data. *SIAM Review*, 51(4):661–703.

Deluca, A. and Corral, á. (2014). Scale invariant events and dry spells for medium-resolution local rain data. *Nonlinear Processes in Geophysics*, 21(2):555–567.

Didan, K. (2015). MOD13Q1 MODIS/Terra Vegetation Indices 16-Day L3 Global 250m SIN Grid V006. *NASA EOSDIS Land Processes DAAC*.

Enku, T., Melesse, A. M., Ayana, E. K., Tilahun, S. A., Abate, M., and Steenhuis, T. S. (2020). Groundwater use of a small Eucalyptus patch during the dry monsoon phase. *Biologia*.

Foken, T. (2017). *Micrometeorology*. Springer Berlin Heidelberg, Berlin, Heidelberg.

Garreaud, R., Barichivich, J., Christie, D. A., and Maldonado, A. (2008). Interannual variability of the coastal fog at Fray Jorge relict forests in semiarid Chile. *Journal of Geophysical Research: Biogeosciences*, 113(G4).

Ghannam, K., Nakai, T., Paschalis, A., Oishi, C. A., Kotani, A., Igarashi, Y., Kumagai, T., and Katul, G. G. (2016). Persistence and memory timescales in root-zone soil moisture dynamics. *Water Resources Research*, 52(2):1427–1445.

Goulden, M. L., Munger, J. W., Fan, S.-M., Daube, B. C., Wofsy, S. C., et al. (1996). Measurements of carbon sequestration by long-term eddy covariance: Methods and a critical evaluation of accuracy. *Global change biology*, 2(3):169–182.

Green, J. K., Konings, A. G., Alemohammad, S. H., Berry, J., Entekhabi, D., Kolassa, J., Lee, J.-E., and Gentine, P. (2017). Regionally strong feedbacks between the atmosphere and terrestrial biosphere. *Nature Geoscience*, 10(6):410–414.

Guswa, A. J., Celia, M. A., and Rodriguez-Iturbe, I. (2002). Models of soil moisture dynamics in ecohydrology: A comparative study. *Water Resources Research*, 38(9):5–1.

Hill, M. J. and Hanan, N. P. (2011). *Ecosystem function in savannas: Measurement and modeling at landscape to global scales.* CRC Press, Boca Raton.

Huxman, T. E., Snyder, K. A., Tissue, D., Leffler, A. J., Ogle, K., Pockman, W. T., Sandquist, D. R., Potts, D. L., and Schwinning, S. (2004). Precipitation pulses and carbon fluxes in semiarid and arid ecosystems. *Oecologia*, 141(2):254–268.

Isaac, P., Cleverly, J., McHugh, I., van Gorsel, E., Ewenz, C., and Beringer, J. (2017). OzFlux data: Network integration from collection to curation. *Biogeosciences*, 14(12):2903–2928.

Jensen, H. J. (1998). *Self-organized criticality: Emergent complex behavior in physical and biological systems*, volume 10. Cambridge University Press.

Kaseke, K. F., Wang, L., and Seely, M. K. (2017). Nonrainfall water origins and formation mechanisms. *Science Advances*, 3(3).

Katul, G. G., Palmroth, S., and Oren, R. (2009). Leaf stomatal responses to vapour pressure deficit under current and CO2-enriched atmosphere explained by the economics of gas exchange. *Plant, Cell & Environment*, 32(8):968–979.

Knapp, A. K., Fay, P. A., Blair, J. M., Collins, S. L., Smith, M. D., Carlisle, J. D., Harper, C. W., Danner, B. T., Lett, M. S., and McCarron, J. K. (2002). Rainfall variability, carbon cycling, and plant species diversity in a mesic grassland. *Science*, 298(5601):2202–2205.

Koster, R. D., Dirmeyer, P. A., Guo, Z., Bonan, G., Chan, E., Cox, P., Gordon, C. T., Kanae, S., Kowalczyk, E., Lawrence, D., Liu, P., Lu, C.-H., Malyshev, S., McAvaney,

B., Mitchell, K., Mocko, D., Oki, T., Oleson, K., Pitman, A., Sud, Y. C., Taylor, C. M., Verseghy, D., Vasic, R., Xue, Y., and Yamada, T. (2004). Regions of strong coupling between soil moisture and precipitation. *Science*, 305(5687):1138–1140.

Kutsch, W. L., Merbold, L., Ziegler, W., Mukelabai, M. M., Muchinda, M., Kolle, O., and Scholes, R. J. (2011). The charcoal trap: Miombo forests and the energy needs of people. *Carbon Balance and Management*, 6(1):5.

Laherrère, J. and Sornette, D. (1998). Stretched exponential distributions in nature and economy: "fat tails" with characteristic scales. *The European Physical Journal B*, 2(4):525–539.

Laio, F., Porporato, A., Ridolfi, L., and Rodriguez-Iturbe, I. (2001). Plants in water-controlled ecosystems: Active role in hydrologic processes and response to water stress: II. Probabilistic soil moisture dynamics. *Advances in Water Resources*, 24(7):707–723.

Leclerc, M. Y. and Foken, T. (2014). *Footprints in micrometeorology and ecology*. Springer, Berlin, Heidelberg.

Li, X., Gentine, P., Lin, C., Zhou, S., Sun, Z., Zheng, Y., Liu, J., and Zheng, C. (2019). A simple and objective method to partition evapotranspiration into transpiration and evaporation at eddy-covariance sites. *Agricultural and Forest Meteorology*, 265:171–182.

Miller, G. R., Cable, J. M., McDonald, A. K., Bond, B., Franz, T. E., Wang, L., Gou, S., Tyler, A. P., Zou, C. B., and Scott, R. L. (2012). Understanding ecohydrological connectivity in savannas: A system dynamics modelling approach. *Ecohydrology*, 5(2):200–220.

Molini, A., Katul, G. G., and Porporato, A. (2009). Revisiting rainfall clustering and intermittency across different climatic regimes. *Water Resources Research*, 45(11).

Nakai, T., Katul, G. G., Kotani, A., Igarashi, Y., Ohta, T., Suzuki, M., and Kumagai, T. (2014). Radiative and precipitation controls on root zone soil moisture spectra. *Geophysical Research Letters*, 41(21):7546–7554.

Nicholson, S. E. (2017). Climate and climatic variability of rainfall over eastern Africa. *Reviews of Geophysics*, 55(3):590–635.

Odongo, V. O., van der Tol, C., Becht, R., Hoedjes, J. C. B., Ghimire, C. P., and Su, Z. (2016). Energy partitioning and its controls over a heterogeneous semi-arid shrubland ecosystem in the Lake Naivasha basin, Kenya: Energy partitioning and its controls over a heterogeneous semi-arid landscape. *Ecohydrology*, 9(7):1358–1375.

Paschalis, A., Fatichi, S., Pappas, C., and Or, D. (2018). Covariation of vegetation and climate constrains present and future T/ET variability. *Environmental Research Letters*, 13(10):104012.

Pellikka, P. K. E., Clark, B. J. F., Gosa, A. G., Himberg, N., Hurskainen, P., Maeda, E., Mwang'ombe, J., Omoro, L. M. A., and Siljander, M. (2013). Chapter 13 - Agricultural expansion and its consequences in the Taita Hills, Kenya. In Paron, P., Olago, D. O., and Omuto, C. T., editors, *Developments in Earth Surface Processes*, volume 16 of *Kenya: A Natural Outlook*, pages 165–179. Elsevier.

Peters, O. and Christensen, K. (2006). Rain viewed as relaxational events. *Journal of Hydrology*, 328(1-2):46–55.

Peters, O., Deluca, A., Corral, A., Neelin, J. D., and Holloway, C. E. (2010). Universality of rain event size distributions. *Journal of Statistical Mechanics: Theory and Experiment*, 2010(11):P11030.

Peters, O., Hertlein, C., and Christensen, K. (2001). A complexity view of rainfall. *Physical Review Letters*, 88(1).

Peters, O. and Neelin, J. D. (2006). Critical phenomena in atmospheric precipitation. *Nature Physics*, 2(6):393–396.

Pollock, M., O'Donnell, G., Quinn, P., Dutton, M., Black, A., Wilkinson, M., Colli, M., Stagnaro, M., Lanza, L., Lewis, E., et al. (2018). Quantifying and mitigating wind-induced undercatch in rainfall measurements. *Water Resources Research*, 54(6):3863–3875.

Porporato, A., Laio, F., Ridolfi, L., Caylor, K. K., and Rodriguez-Iturbe, I. (2003). Soil moisture and plant stress dynamics along the Kalahari precipitation gradient. *Journal of Geophysical Research: Atmospheres*, 108(D3):4127.

Porporato, A., Laio, F., Ridolfi, L., and Rodriguez-Iturbe, I. (2001). Plants in water-controlled ecosystems: Active role in hydrologic processes and response to water stress: III. Vegetation water stress. *Advances in Water Resources*, 24(7):725–744.

Priestley, C. H. B. and Taylor, R. J. (1972). On the assessment of surface heat flux and evaporation using large-scale parameters. *Monthly Weather Review*, 100(2):81–92.

Priestley, M. B. (1981). *Spectral analysis and time series*. Elsevier.

Quansah, E., Mauder, M., Balogun, A. A., Amekudzi, L. K., Hingerl, L., Bliefernicht, J., and Kunstmann, H. (2015). Carbon dioxide fluxes from contrasting ecosystems in the Sudanian Savanna in West Africa. *Carbon Balance and Management*, 10(1).

Rigby, J. R. and Porporato, A. (2010). Precipitation, dynamical intermittency, and sporadic randomness. *Advances in Water Resources*, 33(8):923–932.

Rodríguez-Iturbe, I. and Porporato, A. (2007). *Ecohydrology of water-controlled ecosystems: Soil moisture and plant dynamics*. Cambridge University Press.

Rodriguez-Iturbe, I., Porporato, A., Ridolfi, L., Isham, V., and Coxi, D. R. (1999). Probabilistic modelling of water balance at a point: The role of climate, soil and vegetation. *Proceedings of the Royal Society A: Mathematical, Physical and Engineering Sciences*, 455(1990):3789–3805.

Sankaran, M., Hanan, N. P., Scholes, R. J., Ratnam, J., Augustine, D. J., Cade, B. S., Gignoux, J., Higgins, S. I., Le Roux, X., Ludwig, F., Ardo, J., Banyikwa, F., Bronn, A., Bucini, G., Caylor, K. K., Coughenour, M. B., Diouf, A., Ekaya, W., Feral, C. J., February, E. C., Frost, P. G. H., Hiernaux, P., Hrabar, H., Metzger, K. L., Prins, H. H. T., Ringrose, S., Sea, W., Tews, J., Worden, J., and Zambatis, N. (2005). Determinants of woody cover in African savannas. *Nature*, 438(7069):846–849.

Schemenauer, R. S. and Cereceda, P. (1994). A proposed standard fog collector for use in high-elevation regions. *Journal of Applied Meteorology*, 33(11):1313–1322.

Scholes, R. and Walker, H. (1993). *An African savanna: Synthesis of the Nylsvley study*. Cambridge University Press.

Scholes, R. J. and Archer, S. R. (1997). Tree-grass interactions in savannas. *Annual Review of Ecology and Systematics*, 28(1):517–544.

Schulz, H. M., Thies, B., Chang, S.-C., and Bendix, J. (2016). Detection of ground fog in mountainous areas from MODIS (Collection 051) daytime data using a statistical approach. *Atmospheric Measurement Techniques*, 9(3):1135–1152.

Shuttleworth, W. J. and Wallace, J. S. (1985). Evaporation from sparse crops-an energy combination theory. *Quarterly Journal of the Royal Meteorological Society*, 111(469):839–855.

Stull, R. B. (1988). *An Introduction to boundary layer meteorology*. Atmospheric and Oceanographic Sciences Library. Springer Netherlands.

Tagesson, T., Fensholt, R., Cappelaere, B., Mougin, E., Horion, S., Kergoat, L., Nieto, H., Mbow, C., Ehammer, A., Demarty, J., and Ardö, J. (2016). Spatiotemporal variability in carbon exchange fluxes across the Sahel. *Agricultural and Forest Meteorology*, 226-227:108–118.

Tagesson, T., Fensholt, R., Cropley, F., Guiro, I., Horion, S., Ehammer, A., and Ardö, J. (2015). Dynamics in carbon exchange fluxes for a grazed semi-arid savanna ecosystem in West Africa. *Agriculture, Ecosystems & Environment*, 205:15–24.

Teuling, A. J., Seneviratne, S. I., Williams, C., and Troch, P. A. (2006). Observed timescales of evapotranspiration response to soil moisture. *Geophysical Research Letters*, 33(23).

Veenendaal, E. M., Kolle, O., and Lloyd, J. (2004). Seasonal variation in energy fluxes and carbon dioxide exchange for a broad-leaved semi-arid savanna (Mopane woodland) in Southern Africa. *Global Change Biology*, 10(3):318–328.

Velluet, C., Demarty, J., Cappelaere, B., Braud, I., Issoufou, H. B.-A., Boulain, N., Ramier, D., Mainassara, I., Charvet, G., Boucher, M., Chazarin, J.-P., Oï, M., Yahou, H., Maidaji, B., Arpin-Pont, F., Benarrosh, N., Mahamane, A., Nazoumou, Y., Favreau, G., and Seghieri, J. (2014). Building a field- and model-based climatology of local water and energy cycles in the cultivated Sahel – annual budgets and seasonality. *Hydrology and Earth System Sciences*, 18(12):5001–5024.

Vesala, T., Kljun, N., Rannik, Ü., Rinne, J., Sogachev, A., Markkanen, T., Sabelfeld, K., Foken, T., and Leclerc, M. (2008). Flux and concentration footprint modelling: State of the art. *Environmental Pollution*, 152(3):653–666.

Vico, G. and Porporato, A. (2011). From rainfed agriculture to stress-avoidance irrigation: I. A generalized irrigation scheme with stochastic soil moisture. *Advances in Water Resources*, 34(2):263–271.

Walker, B. H. and Noy-Meir, I. (1982). Aspects of the stability and resilience of savanna ecosystems. In *Ecology of tropical savannas*, pages 556–590. Springer.

Ward, D., Wiegand, K., and Getzin, S. (2013). Walter's two-layer hypothesis revisited: Back to the roots! *Oecologia*, 172(3):617–630.

Welch, P. (1967). The use of fast Fourier transform for the estimation of power spectra: A method based on time averaging over short, modified periodograms. *IEEE Transactions on Audio and Electroacoustics*, 15(2):70–73.

Whitecross, M. A., Witkowski, E. T. F., and Archibald, S. (2016). No two are the same: Assessing variability in broad-leaved savanna tree phenology, with watering, from 2012 to 2014 at Nylsvley, South Africa. *South African Journal of Botany*, 105:123–132.

Whitecross, M. A., Witkowski, E. T. F., and Archibald, S. (2017). Assessing the frequency and drivers of early-greening in broad-leaved woodlands along a latitudinal gradient in southern Africa. *Austral Ecology*, 42(3):341–353.

Wutzler, T., Lucas-Moffat, A., Migliavacca, M., Knauer, J., Sickel, K., Šigut, L., Menzer, O., and Reichstein, M. (2018). Basic and extensible post-processing of eddy covariance flux data with REddyProc. *Biogeosciences*, 15(16):5015–5030.

Yano, J.-I., Liu, C., and Moncrieff, M. W. (2012). Self-organized criticality and homeostasis in atmospheric convective organization. *Journal of the Atmospheric Sciences*, 69(12):3449–3462.

Yin, J., Porporato, A., and Albertson, J. (2014). Interplay of climate seasonality and soil moisture-rainfall feedback. *Water Resources Research*, 50(7):6053–6066.

Zhou, S., Yu, B., Huang, Y., and Wang, G. (2014). The effect of vapor pressure deficit on water use efficiency at the subdaily time scale. *Geophysical Research Letters*, 41(14):5005–5013.